

Chapter 2

Symbolic Dynamics, Poincaré Plot Analysis and Compression Entropy Estimate Complexity in Biological Time Series

Steffen Schulz and Andreas Voss

Abstract Methods from nonlinear dynamics have shown new insights into alterations of the cardiovascular system under various physiological and pathological conditions, and thus providing additional prognostic information. In this chapter prominent complexity methods of non-linear dynamics as symbolic dynamics, Poincaré plot analyses, and compression entropy are introduced and their algorithmic implementations and application examples in clinical trials are provided. Especially, we will give their basic theoretical background, their main features and demonstrate their usefulness in different applications in the field of cardiovascular and cardiorespiratory time series analyses.

2.1 Introduction

Linear time and frequency domain measures are often not sufficient enough to quantify the complex dynamics of physiological systems and their related time series. Therefore, various efforts have been made to apply nonlinear complexity measures to analyze, e.g. the heart rate variability (HRV) [1]. These approaches differ from the traditional time- and frequency domain HRV analyses because they quantify the signal properties instead of assessing only the magnitude or the frequency power of the heart rate time series. They assess the self-affinity of heartbeat fluctuations over multiple time scales (fractal measures); the regularity/irregularity or randomness of heartbeat fluctuations (entropy measures); the coarse-grained dynamics of HR fluctuations based on symbols (symbolic dynamics) and the heartbeat dynamics based on a simplified phase-space embedding [1].

Symbolic dynamics is based on a coarse graining of the dynamics of a signal. The time series (in our cases the ECG or the noninvasively recorded blood pressure curve) are transformed into symbol sequences with symbols of a given alphabet. Some detail information is lost but the coarse dynamic behavior retains and

S. Schulz • A. Voss (✉)

Institute of Innovative Health Technologies IGHT, Ernst-Abbe-Hochschule, Jena, Germany

e-mail: andreas.voss@eah-jena.de

can be analyzed. Depending on the time series we have to define the type and number of symbols. Long time series allow a higher number of symbols (a higher resolution of the dynamics) than short time series. Combining successive symbols into usually called ‘words’, enable the extraction of patterns that represent different system states. In the literature different applications of symbolic dynamics can be found in respect to biological time series analyses, ranging from cardiovascular physiology to the field of neuroscience. In cardiovascular physiology, symbolic dynamics was applied, e.g. for the determination of the sympathovagal balance towards a sympathetic activation and vagal withdrawal during graded orthostatic challenge [2], for monitoring the complexity of the cardiac control [3], to evaluate the maternal baroreflex regulation during gestation [4], to investigate autonomic regulation (cardiorespiratory system) during acute psychosis in patients suffering from paranoid schizophrenia and their healthy first-degree relatives [5], to detect pathological states and improve the risk stratification in cardiology [6]. In the field of neuroscience, symbolic dynamics was applied, e.g. to characterized brain microstates [7], to study the recurrence of microstates during stimulus [8], to detect determinism in perictal intracranial electroencephalographic signals [9], to predict epileptic seizures [10], to assess causal relations between brain signals under different levels of consciousness [11], to detect the development of epileptic seizure [12, 13], and to investigate the central–autonomic coupling in mental disorder [14, 15].

Poincaré plot is a popular HRV analysis tool among clinicians due to its ability to visually represent nonlinear dynamics of HRV. It is a geometrical representation of a time series in a Cartesian plane [16]. Poincaré plot analysis (PPA) represents a nonlinear quantitative technique of phase-space characterization, whereby the shape of the plot can be categorized into functional classes, as suggested by Kamen et al. [17]. PPA allows calculating of heart rate dynamics with trends [17, 18]. The Poincaré plots are two- or three-dimensional graphical representation (scatter plots) of each NN interval or in the time series plotted against subsequent NN intervals. Babloyantz et al. [19] qualitatively and quantitatively analyzed electrocardiograms with Poincaré sections starting in 1988. Typically, PPA shows an elongated cloud of points oriented along the line of identity. Only for graphical illustration an ellipse characterizing the shape of the cloud of points can be drawn in the plot whereas the center of the ellipse is the mean NN value. In general, the Poincaré plot can be evaluated quantitatively through the computation of the SD indexes of the plot [20]. Three indices be calculated: the standard deviation of the instantaneous NN interval variability (minor axis of the ellipse–SD1), the standard deviation of the long term NN interval variability (major axis of the ellipse–SD2) and the axes ratio (SD1/SD2) [21, 22]. Thereby, the Poincaré plot provides information about the beat-by-beat behavior of the heart [21]. Analysis of Poincaré plots revealed increased randomness in beat-to-beat heart rate behavior demonstrated by an increase in the ratio between short-term and long-term HRV suggested that more random short-term heart rate behavior may be associated with a complicated clinical course [23]. This measure has not been used much for risk stratification, but has proved useful for detecting editing problems that significantly influence the calculation of HRV variables [24].

However, it has been shown that the indices SD1 and SD2 of Poincaré plot analysis represent more or less only linear features of the heart rate dynamics [25]. Therefore, new methods of analyzing the Poincaré plots were developed to retain the nonlinear features [26, 27]. Poincaré plot is commonly applied to assess the dynamics of HRV [28–30] and in risk stratification, e.g. for sudden death [26], in patient suffering from dilated cardiomyopathy [31], in cardiac arrhythmia subjects [32, 33].

Among the various approaches that have made progress in the quantification of HRV complexity, entropy measures have gained a significant interest. Shannon entropy, conditional entropy, approximate entropy and sample entropy, respectively are some of the most applied approaches of entropy estimation [34, 35]. Complexity analysis can be performed through the evaluation of entropy and entropy rate. Entropy (e.g., Shannon entropy) calculates the degree of complexity of the distribution of the samples of a signal [34]. For HRV analysis, entropy is not calculated directly over the samples of the biological time series but over patterns of length L (i.e., ordered sequences of L samples). In this case, entropy measures the complexity of the pattern distribution as a function of L [34]. In 1977 Ziv and Lempel [36] developed a universal algorithm for lossless data compression (LZ77) using string-matching on a sliding window. Lossless compression ensures that the original information can be exactly reproduced from the compressed data. The LZ77 algorithm is widely used and implemented in compression utilities such as GIF image compression and WinZip®. LZ77 was modified by Baumert et al. in 2004 [37] to analysis heart rate time series called the compression entropy (H_c). in the field of spontaneous fluctuations of cardiovascular oscillations entropy based methods were applied to investigate fetal development [38], to determine age effects on the autonomic system [39–41], in differentiating pathological states from healthy states [42–46], for monitoring cardiac autonomic function [34, 47], in typifying the effects of a pharmacological treatment [48–51], and in predicting risk [37, 52].

In this chapter, some of the prominent complexity measures and their enhancements as symbolic dynamics, Poincaré plot analyses and compression entropy are introduced and their algorithmic implementations and applications in clinical trials are discussed. Especially, we will give their basic theoretical background, their main features and demonstrate their usefulness in different applications in the field of cardiovascular and cardiorespiratory time series analyses.

2.2 Methods

2.2.1 Symbolic Dynamics

Symbolic dynamics did start with Hadamard's ideas about complex systems in 1898 [53]. The most important result of his work was the simplified description of sequences that can arise in geodesic flows on surfaces of negative curvature. He introduced a finite set of forbidden symbol pairs and defined possible sequences as

those that do not contain any forbidden symbol pair. Later on, Morse and Hedlund [54] used this method in 1938 to prove the existence of periodic and other dynamics in different classical dynamical systems. They showed that in many circumstances such a finite description of a systems dynamics is possible and performed their investigations by finding interesting sequences satisfying the constraints defined by the corresponding symbolic dynamical system.

In 1983, Aizawa [55] reported that symbolic dynamics could be systematically constructed near the onset point of chaos by taking into account the topological similarity of the Lorenz map and Hao [56] investigated symbolic dynamics applying sequences of two, three and more letters. Although symbolic dynamics was originally developed as a method to study basic structures and behavior of dynamical systems, the methods and the technology have found significant application in various fields of sciences. Some of the major fields for applications of symbolic dynamics are linear algebra, data storage (coding), data transmission (information theory), data analysis and processing as well as life sciences. One of the first life science applications were from Paulus et al. [57] who applied symbolic dynamics in animal experiments.

The research groups of Kurths and Voss were the first who introduced symbolic dynamics into heart rate variability analysis in 1993 [58] and later 1995 [59] and 1996 [6] developing special optimized measures for analysis of the heart rate dynamics. The introduced measures were finally validated in risk stratification based on data from 572 patients after myocardial infarction [60].

The analysis of symbolic dynamics has been proven to be sufficient for the investigation of complex systems and describes dynamic aspects within time series [6, 61, 62]. The concept of symbolic dynamics is based on a coarse-graining of the dynamics. To classify dynamic changes within, e.g. heart rate time series RR_1, RR_2, \dots, RR_n they were transformed into a symbol sequence $s_1, \dots, s_n, s_i \in A$ with four symbols from the alphabet $A = \{0, 1, 2, 3\}$ (Fig. 2.1). There, according to the transformation rules in equation μ is the mean beat-to-beat interval (RR), a is a special scaling parameter equal to 0.1 and RR_n is the beat-to-beat interval at the time point n .

$$0 : \mu < RR_i \leq (1 + a) * \mu$$

$$1 : (1 + a) * \mu < RR_i < \infty$$

$$2 : (1 - a) * \mu < RR_i \leq \mu$$

$$3 : 0 < RR_i \leq (1 - a) * \mu$$

where $i = 1, 2, 3, \dots$

In this way some detailed information is lost but the more general dynamic behavior can be analyzed [59]. It is important to mention that small changes

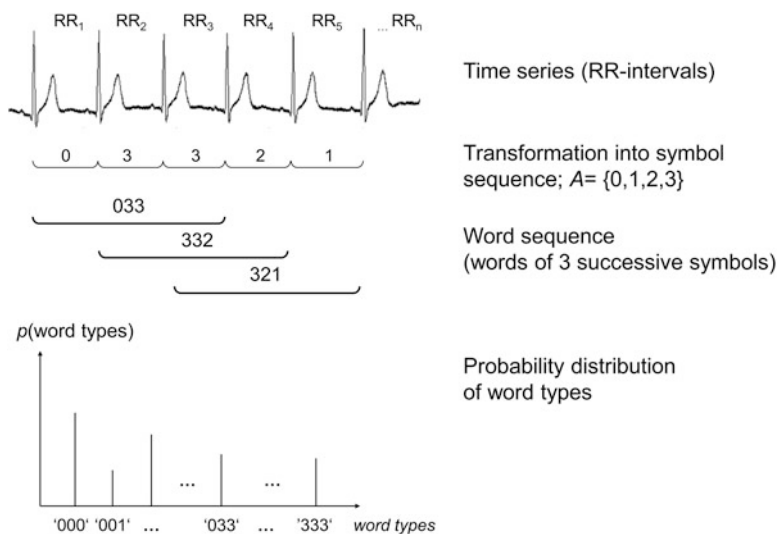


Fig. 2.1 Basic principle of symbolic dynamics analyses based on RR-intervals

of the threshold parameters a and μ do not significantly influence the analysis results. There are several quantities that characterize such symbol strings. We obtain 64 different word types (000, 001, ..., 333) using three successive symbols from the alphabet A to characterize symbol strings. The Shannon [63] and Rényi [64] entropies calculated from the distribution of word types $p(\text{word types})$ are suitable measures to quantify the dynamic behavior of heart beat time series and their complexity. High values of these entropies refer to higher complexity in the investigated heart beat time series, vice versa.

An example of word type distributions (histograms) obtained from BBI time series of white noise, a healthy subject, a patient suffering from coronary heart disease and a patient suffering from atrial fibrillation are shown in Fig. 2.2.

The Shannon entropy (H_{Shannon}) is the classical measure of information and is defined as [59]

$$H_{\text{Shannon}} = -\sum_{i=1}^k p_i \log_2 p_i$$

where p is the probability distribution of every single word type and k ($=64$) is the total number of word types. The Rényi entropy generalizes the Shannon entropy and is estimated from α -weighted probabilities distributions (for HRV analysis often an α value of 0.25 or 4 is in use) by [59]

$$H_{\text{Renyia}} = -\frac{1}{\alpha} \log_2 \sum_{i=1}^k p_i^\alpha.$$

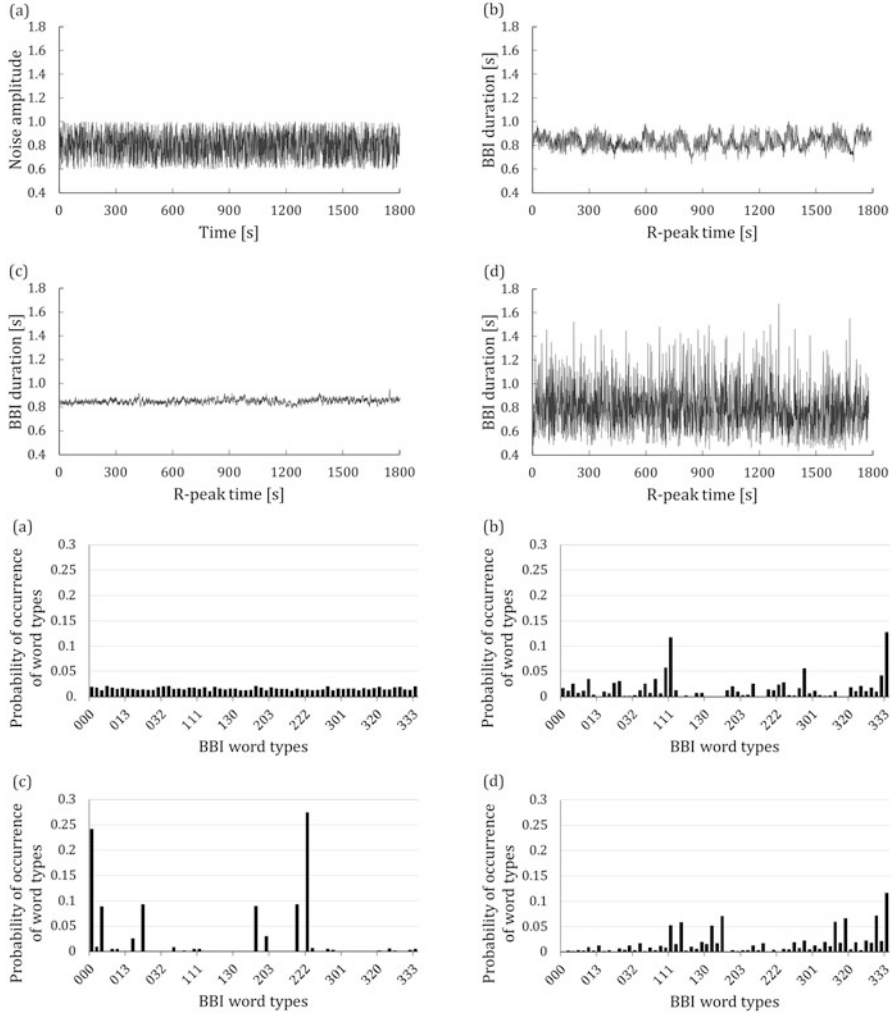


Fig. 2.2 Symbolic dynamics: Tachograms and word distributions (histograms) obtained from BBI time series applying symbolic dynamic analysis of (a) white noise, (b) a healthy subject, (c) a patient suffering from coronary heart disease and (d) a patient suffering from atrial fibrillation. (BBI = beat-to-beat intervals)

The word type distribution p differs between short (30 min) and long term (24 h) measures in healthy subjects as well as patient with ischemic cardiomyopathy.

Another procedure which based on word distribution is to count the number of words with length 3 that seldom or never occur so called ‘forbidden words’

$$p_{WTi} = \frac{n_{WTi}}{N} < 0.001$$

with p_{WTi} as probability of word types i occurrence, N is the number of all words and n_{WTi} is the number words in type i defined by $n_{WTi} = \sum_j W_{ij}$ with W_{ij} as single word j of word type i .

A high number of forbidden words reflect a reduced dynamic behavior in the heart beat time series. If the heart beat time series is highly complex in the Shannonian sense, only a few forbidden words are found. Words with a probability less than 0.1% were counted. The parameter 'wsdvar' is a measure of heart rate time series variability depending on a word sequence. The resulting word sequence $\{w_1, w_2, w_3, \dots\}$ is transformed into a sequence $\{\bar{S}_1, \bar{S}_2, \bar{S}_3, \dots\}$, where 'wsdvar' is defined as the standard deviation of this sequence \bar{S}_i . Further, a high percentage of word, which consist only of symbols '0' and '2' define the parameter 'wpsum02' that is a good measure of decreased HRV, conversely a measure of increased HRV is given by 'wpsum13' (symbols '1' and '3').

In 1999 Wessel et al. [65] applied a new method of long-term symbolic dynamics in patients with dilated cardiomyopathy. They investigated 24 h heart beat time series which allow a higher number of symbols than short-term time series. For the transformation of the time series they used five symbols from the alphabet $A = \{0, 1, 2, 3, 4, 5\}$ instead of four symbols. Thereby, a higher resolution of the analysis was given. The time series are subdivided into short word sequences (bins) of word length k . The number of word types depends on the number of RR-intervals within the time series and is given by word types = (number of symbols)^{word length}.

For example for a 24 h recording (mean heart rate: 80 bpm, number of symbols = 6, word length = 4, word types = 1296) the time series has a length N of 115,200 RR-intervals in the tachogram, so that there are about 89 words in each bin.

$$p(w_k) = \frac{N}{wordtypes} = \frac{115199}{6^4} = 89$$

The accuracy of the word distribution will be reduced by too few words per bin. Voss et al. [6] defined a heuristic basis of 20 as the averaged minimal number of words per bin.

Calculating the percentage of words consisting only of a unique type of symbols is other approach to find epochs of low or high variability. In this way 6 successive symbols of a simplified alphabet [6], consisting only of symbols '0' or '1', $A = \{0, 1\}$ were observed. Here the symbol '0' stands for a difference between two successive beats lower than a special limit (5, 10, 20, 50, and 100 msec) whereas '1' represents those cases where the difference between two successive beats exceeds this special limit:

$$'1' : |RR_n - RR_{n-1}| \leq limit$$

$$'0' : |RR_n - RR_{n-1}| < limit$$

Words consisting only of a unique type of symbol (either all ‘0’ or all ‘1’) were counted. For low variability (‘plvar’) of sequences containing six consecutive ‘0’ were assessed, whereas for high variability (‘phvar’) six consecutive ‘1’ were evaluated. There, an increase of ‘000000’ (plvar5, plvar10, plvar20) sequences resulting in increased values of ‘plvar’ and a decrease in ‘111111’ (plvar20, plvar50, plvar100) sequences leading to reduced values of ‘phvar’ indicate reduced system complexity.

In 2001 Porta et al. [34] introduced a modified procedure of symbolic dynamics. Here the length of the RR-intervals was limited to 300 beats. The full range of the sequences was uniformly spread on 6 levels (0 to 5), and patterns of length $L = 3$ were constructed [66]. All patterns with $L = 3$ were grouped without any loss into four families. These were: (1) patterns with 0 variations—0 V, (2) patterns with 1 variation—1 V, (3) patterns with 2 like variations—2LV and (4) patterns with 2 unlike variations—2UV. The rates of occurrence of these patterns will be indicated as 0 V%, 1 V%, 2 LV% and 2 UV% [67].

To obtain more detailed information about the dynamics of heart rate some new pattern families were introduced [44, 68]: ‘ramp’/‘ASC’ (three successive symbols form an ascending ramp), ‘decline’/‘DESC’ (three successive symbols form a descending ramp), ‘PEAK’ (second symbol is larger than the other two symbols forming a peak) and ‘VAL’ (second symbol is smaller than the other two symbols forming a valley).

A further extension of the classical symbolic dynamic approach represents the segmented short term symbolic dynamic. The segmented short-term symbolic dynamics (SSD) was introduced in order to describe nonlinear aspects within long-term RR time series applying a 24-hour segmentation algorithm in an enhanced way [45, 69]. Therefore, the related time series were segmented in both 1 min overlapping and non-overlapping time windows of 15 min, 30 min or 60 min duration. Within each of these windows a symbol- and word transformation were performed in accordance to the classical symbolic dynamics approach with the scaling parameter $a = 0.1$ [58]. For each segment ($s = 1 \dots S$, S —number of segments) from the 24-hour interval time series, several parameters based on the word distribution were estimated:

- $pW000_s$ to $pW333_s$ – Probability of occurrence of each word type (000,001, ..., 333) within the interval time series;
- $pTH1_s$ to $pTH20_s$ —Number of words with a probability higher than a threshold pTH (1–20%);
- m_pW000 to m_pW333 as the mean values and s_pW000 to s_pW333 as the standard deviations of the parameters $pW000_s$ to $pW333_s$ and $pTH1_s$ to $pTH20_s$;
- $Shannon_pWxxx$ —The Shannon entropy calculated from the distribution of each single word type ‘xxx’ over all windows were estimated as a suitable measure to quantify the dynamic behavior and the complexity of the word type occurrence in the windowed time series.

Cysarz et al. [3, 70] investigated different approaches for the transformation of the original time series to the symbolic time series. They investigated three different

transformation methods as: (1) symbolization according to the deviation from the average time series (σ -method), (2) symbolization according to several equidistant levels between the minimum and maximum of the time series (max-min-method), (3) binary symbolization of the first derivative of the time series (binary Δ -coding-method). Each method was applied to cardiac interbeat interval series RR_i and its difference ΔRR_i , and the occurrence of short sequences (“words”) of length $k = 3$ were analyzed. The sequences of length k were categorized according to their amount of variations between successive symbols as proposed by Porta et al. [34]. They could show that all methods are capable of reflecting changes of the cardiac autonomic nervous system, here during head-up tilt. In addition, they demonstrated that changes of cardiovascular regulation during pharmacological challenges can be assessed by the analysis of symbolic dynamics derived from the RR interval series independently of the specific symbolic transformation rule. Finally, they concluded that the ‘standard’ setting of the different parameters of the investigated methods yield reasonable results and can be used in future clinical studies. However, more refined results could be obtained by an optimized setting of the parameters. Especially, the impact of the parameters should be investigated in more details.

Recently methods have been developed to analyze couplings in dynamic systems. In the field of medical analysis of complex physiological system is a growing interest in how insight may be gained into the interaction between regulatory mechanisms in healthy and diseased persons. For the analyses of the physiological regulatory systems (cardiovascular, cardiorespiratory) as well as the quantification of their interactions, a variety of linear as well as nonlinear methods ranging from parametric models in the time- or in the frequency domain to model-free approaches in the information domain have been proposed [71]. Linear methods are partly insufficient to quantify nonlinear structures and the complexity of physiological systems (time series)—the joint symbolic dynamics (JSD) [4, 72] and high resolution joint symbolic dynamics (HRJSD) [73] overcomes the limitations.

2.2.1.1 Joint Symbolic Dynamics – (JSD)

In 2002, Baumert et al. [4] introduced the method of joint symbolic dynamics (JSD) to investigate the nonlinear interaction between blood pressure and heart beat time series in a more complex way. This method based on the analysis of dynamic processes by means of symbols [6] and allows a simplified quantification of the dynamics of two time series. Therefore, both time series were transformed into symbol sequences of different words. The symbol sequences consist only of ‘0’ and ‘1’, increasing values are coded as ‘1’ and decreasing and unchanged values are coded as ‘0’, respectively, and words of length 3 were formed using a shift of one symbol in time series. Following indices were estimated:

- Normalized probabilities of all single word type ($k = 64$) occurrences were computed as (JSD1-JSD64) using an 8x8 word distribution density matrix;

- SumSym—Symmetric word types where the pattern in both time series are equal (for cardiovascular time series this index reflecting baroreflex-like response patterns);
- SumDiam—Diametric word types, where the response of the first time series to second time series changes is asymmetric (for cardiovascular time series this index reflecting the opposite of baroreflex; patterns);
- JSD_{Shannon}—The Shannon entropy computed over all 64 word types in the word distribution matrix.

With the JSD method a rough assessment of the overall short-term bivariate interactions can be obtained. In 2011, Kabir et al. [74] proposed a tertiary symbolization scheme and quantified the relative frequency of word types, capturing RSA patterns and thereby adding physiological a-priori knowledge to the analysis. To address the issue of different frequencies between cardiac and respiratory oscillators, Hilbert transformation was introduced to obtain the instantaneous respiratory phase (RP) sampled at the R peak in ECG, yielding beat-to-beat symbol sequences of changes in RR interval and respiratory phase. [75].

2.2.1.2 High Resolution Joint Symbolic Dynamics – (HRJSD)

HRJSD was introduced to quantify the effect of antipsychotics on cardiovascular couplings in patients suffering from acute schizophrenia [73]. The idea of HRJSD is to classify frequent deterministic patterns lasting three beats (symbols). The HRJSD approach enables the classification and characterization of short-term cardiovascular regulatory bivariate coupling patterns which are dominating the interaction generated by the autonomic nervous system. In contrast to other coupling approaches HRJSD emphasizes a clear characterization how the couplings are composed by the different regulatory aspects of the autonomic nervous system. HRJSD based on the classical JSD [4] analyzing dynamic processes by means of symbols. HRJSD has been successful applied to investigate cardiovascular, cardiorespiratory and central-autonomic couplings [5, 14, 76, 77].

In short, HRJSD works in the way that both time series (e.g. heart rate (BBI) and respiratory frequency (RESP)) were transformed into symbol sequences (word length of 3) applying 3 symbols $A = \{0,1,2\}$ and a threshold level l_{BBI} and l_{RESP} for symbol (Fig. 2.3).

Threshold levels for symbol transformation are: no threshold (similar to JSD); the spontaneous baroreflex sensitivity based on the sequence technique [78, 79] and 25% of the standard deviation of the investigated time series as an adapted threshold to the individual physiological dynamic variability.

Thereby, X represents a bivariate sample vector with x_{BBI} and x_{RESP} as the n beat-to-beat values of BBI and RESP, respectively.

$$X = \left\{ \begin{bmatrix} x_n^{BBI} & x_n^{RESP} \end{bmatrix}^T \right\}_{n=0,1,\dots} \quad x \in R$$

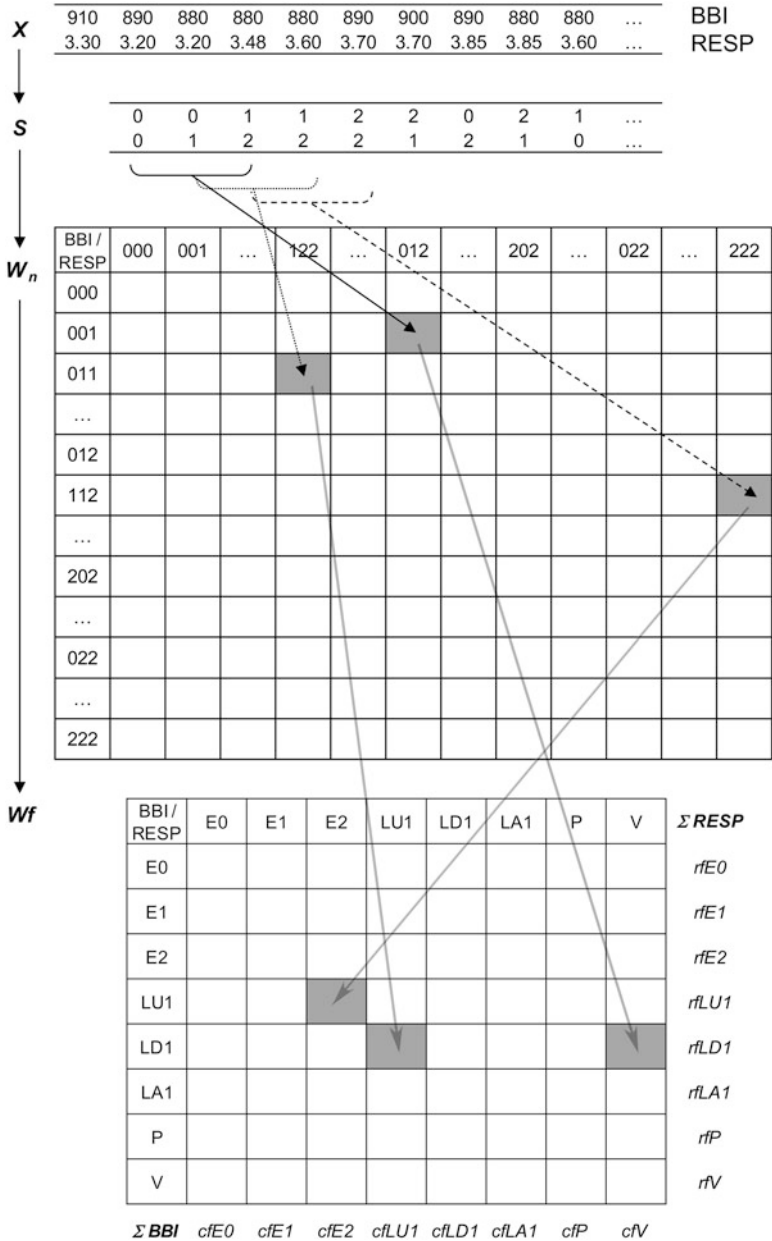


Fig. 2.3 Basic principle of High Resolution Joint Symbolic Dynamics (HRJSD) analysis: (top) Transformation of the bivariate sample vector X (BBI = beat-to-beat intervals [ms]; RESP = respiratory frequency [s]) into the bivariate symbol vector S ('0': decreasing values; '1': equal values and '2': increasing values); (middle): Word distribution density matrix W_n (27x27); (bottom): Word pattern family distribution density matrix W_f (8x8) with 8 pattern families wf , rf_{BBI} row sum of specific word family and cf_{RESP} column sum of specific word family

For the symbol transformation X is afterwards transformed into a bivariate symbol vector S defined as

$$S = \left\{ [s_n^{BBI}, s_n^{RESP}]^T \right\}_{n=0,1,\dots} \quad s \in 0, 1, 2$$

with the following definitions

$$s_n^{BBI} = \begin{cases} 0 : (x_{n+1}^{BBI} - x_n^{BBI}) < -l^{BBI} \\ 1 : -l^{BBI} \leq (x_{n+1}^{BBI} - x_n^{BBI}) \leq l^{BBI} \\ 2 : (x_{n+1}^{BBI} - x_n^{BBI}) > l^{BBI} \end{cases}$$

$$s_n^{RESP} = \begin{cases} 0 : (x_{n+1}^{RESP} - x_n^{RESP}) < -l^{RESP} \\ 1 : -l^{RESP} \leq (x_{n+1}^{RESP} - x_n^{RESP}) \leq l^{RESP} \\ 2 : (x_{n+1}^{RESP} - x_n^{RESP}) > l^{RESP} \end{cases}.$$

Symbol sequences S was subdivided into short words (bins) w_k of length $k = 3$. Three symbols led to 27 different word types for BBI (w_{BBI}) and RESP (w_{RESP}) (word types ranging from: 000,001, ..., 221,222). Symbol sequences with increasing values were coded as “2”, decreasing values were coded as ‘0’ and unchanging (no variability) values were coded as ‘1’. All single word types $w_{BBI,RESP}$ (total number of all word type combinations $27 \times 27 = 729$) were afterwards grouped into eight pattern families wf whereby the sum of probabilities of all single word families’ occurrences $p(wf)$ was normalized to 1 (Fig. 2.3).. The 8 pattern families (E0, E1, E2, LU1, LD1, LA1, P, V) represent different aspects of autonomic modulation (strong and weak increase/ decrease, no variability, alternations) and were sorted into an 8x8 pattern family density matrix Wf resulting in 64 cardiorespiratory coupling patterns. The pattern definition (Fig. 2.4) is as follows:

- E0, E1 and E2—No variation within the word consisting of three symbols of type ‘0’, ‘1’ and ‘2’, respectively.
- LU1 and LD1—One variation within the word consisting of two different symbols with low increasing behavior (LU1) and low decreasing behavior (LD1) of BBI and SYS.
- LA1—One variation within the word consisting of two different alternating symbols of type ‘0’ and ‘2’ with an increasing-decreasing behavior of BBI and SYS.
- P and V—Three variations within the word consisting of three different symbols with peak-like behavior (P) and with valley-like behavior (V) of BBI and SYS.

Besides the 64 coupling patterns, 8 pattern families for BBI and RESP the sum of each ($n = 8$) column cf_{RESP} ($cfE0$, $cfE1$, $cfE2$, $cfLU1$, $cfLD1$, $cfLA1$, cfP , cfV), the

Word family	Definition	Effect on		
		HR	SYS/RESP	EEG
E0	no variation within the word consisting of three symbols of type '0' (decreasing BBI, SYS & EEG behavior; '000')	↑	↓	↓
E1	no variation within the word consisting of three symbols of type '1' (unchanging BBI, SYS & EEG behavior; '111')	→	→	→
E2	no variation within the word consisting of three symbols of type '2' (increasing BBI, SYS & EEG behavior; '222')	↓	↑	↑
LU1	one variation within the word consisting of two different symbols with low increasing behavior of BBI, SYS & EEG ('122', '022', '112', '221', '220', '211', '121', '212')	↘	↗	↗
LD1	one variation within the word consisting of two different symbols with low decreasing behavior of BBI, SYS & EEG ('011', '001', '002', '110', '100', '200', '010', '101')	↗	↘	↘
LA1	one variation within the word consisting of two different alternating symbols of type '0' and '2' with an increasing-decreasing behavior of BBI, SYS & EEG ('020', '202')	↗↘	↗↘	↗↘
P	three variations within the word consisting of three different symbols with peak-like behavior of BBI, SYS & EEG ('120', '201', '210')	↘↗	↘↗	↘↗
V	three variations within the word consisting of three different symbols with valley-like behavior of BBI, SYS & EEG ('021', '102', '012')	↗↘	↗↘	↗↘

Fig. 2.4 Definition of 8 pattern families of High Resolution Joint Symbolic Dynamics (HRJSD) (HR = heart rate; BBI = beat-to-beat intervals; SYS = systolic blood pressure; RESP = respiratory frequency; EEG: mean power EEG time intervals in relation to BBI)

sum of each ($n = 8$) row rf_{BBI} ($rfE0$, $rfE1$, $rfE2$, $rfLU1$, $rfLD1$, $rfLA1$, rfP , rfV) and the Shannon entropy ($HRJSD_{Shannon}$) of Wf as a measure of the overall complexity of the coupling (can be determined).

$$HRJSD_{Shannon} = -\sum_{i,j=1}^8 [p(wf_{ij}) \log_2 p(wf_{ij})]$$

Being a unique feature of the HRJSD approach in contrast to other coupling approaches is the identification of different physiological regulatory patterns generated by the interplay of the involved physiological regulatory systems. From the aspect of biomedical signal processing based on symbolic analysis, the HRJSD approach, based on a redundancy reduction strategy and grouping of single-word types into eight pattern families, enables a detailed description and quantification of bivariate couplings. As a further unique feature in contrast to the classical JSD approach and other coupling approaches [15, 80] HRJSD emphasizes a clear characterization of how the couplings are composed, with regard to the different regulatory aspects of the interacting systems. To summarize, HRJSD approach creates a bridge between univariate and bivariate symbolic analyses, allowing the quantification and classification of deterministic regulatory bivariate coupling patterns depending on the experimental conditions at hand [73].

As a further enhancement on joint symbolic dynamics analyses we have recently extended the HRJSD approach to analyses three signals for multivariate analyses (mHRJSD). Thereby, X represents a trivariate sample vector with e.g. x_{BBI} , y_{SYS} and z_{RESP} as the n beat-to-beat values of BBI, SYS (systolic blood pressure) and RESP, respectively.

$$X = \left\{ \left[x_n^{\text{BBI}}, y_n^{\text{SYS}}, z_n^{\text{RESP}} \right]^T \right\}_{n=0,1,\dots} \quad x \in R$$

In mHRJSD X is afterwards transformed into a trivariate symbol vector S defined as

$$S = \left\{ \left[s_n^{\text{BBI}}, s_n^{\text{SYS}}, s_n^{\text{RESP}} \right]^T \right\}_{n=0,1,\dots} \quad s \in 0, 1, 2.$$

8 pattern families (E0, E1, E2, LU1, LD1, LA1, P, V) were derived from each of the three time series and sorted into an $8 \times 8 \times 8$ pattern family density matrix W_f leading to multivariate coupling pattern. As an example, the pattern family ‘E0’ from BBI time series is coupled with the eight pattern families from SYS and 8 from RESP as: BBI-E0/SYS-E0/RESP-E0, BBI-E0/SYS-E0/RESP-E1, BBI-E0/SYS-E0/RESP-E2, BBI-E0/SYS-E0/RESP-LU1, ..., BBI-E0/SYS-V/RESP-V. Thus, the pattern family ‘E0’ (BBI-E0/SYS-E0/RESP-E0) contains word types that consist only of the ‘0’ symbol. On one hand, this means that BBI decreases over three values and which were therefore coded by ‘0’ three times (representing an increase of the mean heart rate over three values) whereas on the other hand, SYS values increases and RESP values decrease over three values.

2.2.1.3 Joint Conditional Symbolic Analysis – (JCSA)

In 2015, Porta et al. [81] extended the short-term symbolic dynamics procedure [34] to a bivariate and multivariate ones—the joint symbolic analysis (JSA) and the joint conditional symbolic analysis (JCSA). In principle, they created for two time series (x , y) for each time series separately the pattern 0 V, 1 V, 2LV and 2UV. Afterwards, joint patterns by associating one pattern of x and one of y were formed. Thereby, coordinated activity between x and y was investigated by considered introducing two categories: (i) coordinated (C) joint Scheme (0 V–0 V, 1 V–1 V, 2LV–2LV and 2UV–2UV) and (ii) uncoordinated (UNC) joint scheme with different classes (e.g. 1 V and 2UV). The percentage of 0 V–0 V, 1 V–1 V, 2LV–2LV and 2UV–2UV patterns (i.e. 0 V–0 V%, 1 V–1 V%, 2LV–2LV% and 2UV–2UV%) was computed by dividing their amount by the number of C ones and, then, by multiplying the result by 100. In the case of JCSA, x and y were conditioned on a third signal s (e.g. the respiratory phase: inspiration (INSP) and expiration (EXP) phases, the transitions from INSP to EXP (INSP–EXP) and vice

versa (EXP–INSP) over s). Thus, e.g. the coordinated pattern 0 V–0 V, 1 V–1 V, 2LV–2LV and 2UV–2UV whose symbols are associated with events all occurring in the inspiratory (INSP) phase are classified as 0 V–0 V|_{INSP}, 1 V–1 V|_{INSP}, 2LV–2LV|_{INSP} and 2UV–2UV|_{INSP}. Analogously, they defined 0 V–0 V|_{EXP}, 1 V–1 V|_{EXP}, 2LV–2LV|_{EXP} and 2UV–2UV|_{EXP} as the joint patterns whose values are all linkable to the expiratory (EXP) phase. The percentage of the 0 V–0 V, 1 V–1 V, 2LV–2LV and 2UV–2UV patterns occurring in the INSP phase (i.e. 0 V–0 V%|_{INSP}, 1 V–1 V%|_{INSP}, 2LV–2LV%|_{INSP} and 2UV–2UV%|_{INSP}) were computed by dividing the number of the 0 V–0 V, 1 V–1 V, 2LV–2LV and 2UV–2UV patterns occurring in the INSP phase by the number of coordinated patterns (C) occurring in the INSP phase and, then, by multiplying the results by 100 [81, 82].

2.2.1.4 Symbolic Coupling Traces – (SCT)

A further JSD extension represents the symbolic coupling traces (SCT) introduced by Wessel et al. [83]. SCT based on the analysis of structural patterns and enables the detection of the direction (bidirectional) of time-delayed couplings in short-term bivariate time series. Using the classical JSD algorithm two time series $x(t)$ and $y(t)$ were transformed into symbol sequences $s_x(t)$ and $s_y(t)$ using also the alphabet $A = \{0,1\}$ and afterwards series of word $w_x(t)$ and $w_y(t)$ of length $l = 3$ were formed. In contrast to JSD a delay-time probability matrix $\Pi(\tau) = (p_{ij}(\tau))$ was estimated describing how word W_i would occur in w_x at time t and W_j would occur in w_y at time $(t + \tau)$ with p_{ij} as the joint probabilities of the words. For the quantification of SCT used only the symmetric and diametric traces of the bivariate word distribution matrix (BWD), thereby excluding random effects and including only significant coupling information whereby following measures can be calculated:

The trace T of the matrix $\Pi(\tau)$ defined as

$T(\tau) = \sum_i p_{ii}(\tau)$ represents the fraction of both time series, which are structurally equivalent to each other at lag τ ;

The trace $\bar{T}(\tau)$ of the matrix $\Pi(\tau)$ defined as

$\bar{T}(\tau) = \sum_{i=1, \dots, d} p_{i, d+1-i}(\tau)$ describing the fraction of both signals, which are structurally diametric at lag τ (d is the number of different patterns). Both parameters vary from 0 to 1 and comprise the diagonals of the BWD only. Finally, the difference $\Delta T = T - \bar{T}$ can be calculated to determine the exact detection of lags (delayed couplings) between two time series. Thereby, T only captures influences which preserve the structure of the transmitted pattern of dynamics (symmetrical influences) and \bar{T} only quantifies influences which inverts the dynamical structure of the driver (diametrical influence) [84]. The lags τ should be limited to $20 \leq \tau \leq 20$ (sampling units) in order to focus on short time-delayed dependencies only. The main advantages of SCT are its ability to detect delayed coupling (time lags), its applicability to moderately noisy time series (< 10 dB) and its insensitivity to non-stationarities. [71, 85].

2.2.1.5 Specifics and Restrictions

SD: Detailed information will be lost; outliers (ectopic beats and noise) influence symbol strings; the accuracy of the word distribution will be reduced by too few words per bin (heuristic basis of 20 as the averaged minimal number of words per bin are needed [6]; no stationarity required; short- and long term time series analyses; only short-term fluctuations can be investigated depending on the word length (3–6 symbols).

JSD/HRJSD: Coarse-graining without any information about information flow; based on a bivariate redundancy reduction strategy to group single word types into eight pattern families; allowing a detailed quantification and classification of deterministic regulatory bivariate coupling patterns depending on experimental conditions; no stationarity required; short- and long term time series analyses; only short-term fluctuations can be investigated depending on the word length (3 symbols).

SCT: High noise levels (>10 dB) influence detection of delayed coupling; critical significance level has to be calculated; no stationarity required; short- and long term time series analyses; only short-term fluctuations can be investigated depending on the word length (3 symbols).

2.2.2 Poincaré Plot Analyses

The Poincaré plot analysis (PPA) is a method that allows calculating of heart beat dynamics with trends [17, 18, 86]. The Poincaré plots are two-dimensional graphical representation (scatter plots) of each RR-interval or in the time series plotted against the subsequent RR-interval.

It provides a visual and quantitative analysis of RR-interval sequences. Babloyantz et al. [19] qualitatively and quantitatively analyzed electrocardiograms with Poincaré sections in 1988.

Thereby, the shape of the plot, that is assumed to be influenced by changes in the vagal and sympathetic modulation, can be used to classify the sequence into one of several classes. The plots provide detailed beat-to-beat information on the behavior of the heart [17]. Typically, PPA shows an elongated cloud of points oriented along the line of identity. Only for graphical illustration an ellipse characterizing the shape of the cloud of points can be drawn in the plot whereas the center of the ellipse is the mean RR value. In general, three indices are calculated from the Poincaré plots: the standard deviation of the instantaneous BBI variability (minor axis of the ellipse— $SD1$), the standard deviation of the long term BBI variability (major axis of the ellipse— $SD2$) and the axes ratio ($SD1/SD2$) [21, 22, 86].

The level of short-term variability can be quantified by $SD1$ and the level of long-term variability is given by $SD2$. $SD1$ and $SD2$ are calculated using:

$$x_n = (x_1, x_2, \dots, x_{N-1}) \text{ and } x_{n+1} = (x_2, x_3, \dots, x_N)$$

$$SD1 = \sqrt{\frac{VAR \frac{x_n - x_{n+1}}{\sqrt{2}}}{\sqrt{2}}}$$

$$SD2 = \sqrt{\frac{VAR \frac{x_n + x_{n+1}}{\sqrt{2}}}{\sqrt{2}}},$$

where VAR is the variance, x_n is a time series with $n = 1, \dots, N-1$ (N -length of time series) and x_{n+1} is the same time series shifted by one.

Laitio et al. [23] showed that an increased $SD1/SD2$ ratio was the most powerful predictor of postoperative ischemia. Stein et al. [87] also demonstrated that an increased $SD1/SD2$ ratio had the strongest association with mortality. Further, Mäkikallio et al. [88] found for healthy subjects $SD1/SD2 \approx 0.2$, for post infarction patients with ventricular tachyarrhythmia $SD1/SD2 \approx 0.3$ and for patients with a previous myocardial infarction who had experienced ventricular fibrillation $SD1/SD2 \approx 0.6$. Voss et al. [61] found a significant reduced value for $SD1 \approx 15$ in patient with dilated cardiomyopathy in comparison to healthy subjects $SD1 \approx 24$. Furthermore, Voss et al. showed [89] that the cloud of the Poincaré plot are characterized by high variability for healthy subjects; reduced to a narrow distribution of the cloud for patients at high risk; and arrhythmias producing separate clouds in the Poincaré plot. Arrhythmias can be easily visually detected connecting each single point of the cloud by trajectories. Moreover, they presented first attempts of lagged- and three-dimensional Poincaré plots.

An example of standard Poincaré plots obtained from BBI time series of white noise, a healthy subject, a patient suffering from coronary heart disease and a patient suffering from atrial fibrillation are shown in Fig. 2.5.

2.2.2.1 Segmented Poincaré Plot Analysis – (SPPA)

The SPPA approach was introduced by Voss et al. [26] as a nonlinear approach of phase-space characterization for the nonlinear quantification of NN time series based on the traditional Poincaré plot analysis. Thereby, the cloud of points is segmented into 12×12 equal rectangles whose size depends on the standard deviations $SD1$ (height) and $SD2$ (width) of BBI, SYS and DIA NN time series of the Poincaré plot.

Thereby, the cloud of points presented by PPA is then rotated $\alpha = 45$ degrees around the main focus of the plot allowing for a simplified $SD1/SD2$ adapted probability-estimating procedure (Fig. 2.6). Starting from the main focus of the plot, a grid of 12×12 rectangles is drawn into the plot [27]. For the estimation of the single probabilities (p_{ij}) within each rectangle the number of points within every rectangle is counted and normalized by the total number of all points. Based on these single probabilities all row (i) and column (j) probabilities are calculated by summation of the related single probabilities as:

- SPPA_r_i = single probability of each row with $i = 1-12$,
- SPPA_c_j = single probability of each column with $j = 1-12$.

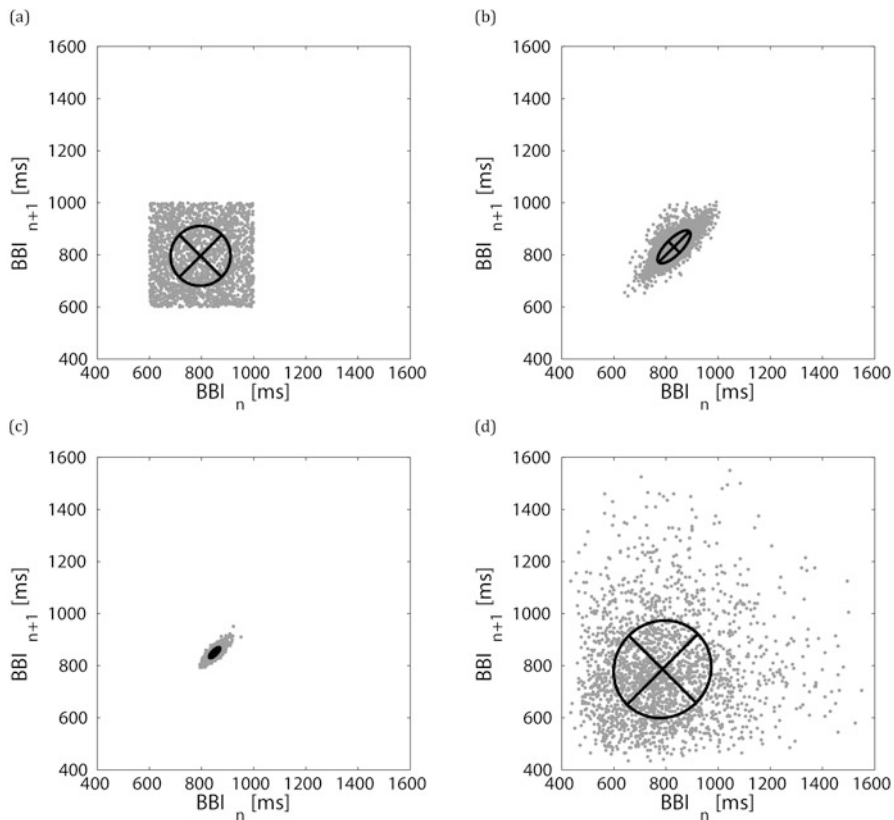


Fig. 2.5 Poincaré plot analysis: Standard Poincaré plots of BBI time series of (a) white noise, (b) a healthy subject, (c) a patient suffering from coronary heart disease and (d) a patient suffering from atrial fibrillation. (BBI = beat-to-beat intervals)

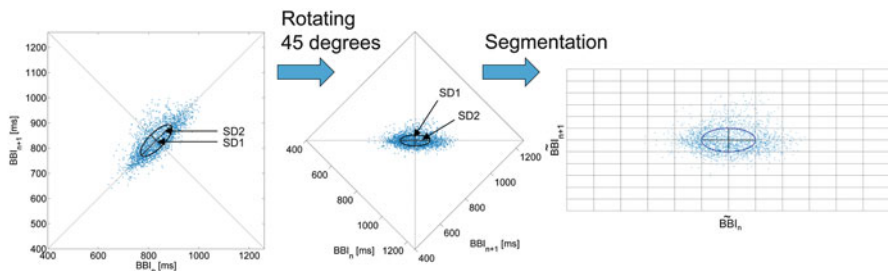


Fig. 2.6 Basic principle of segmented Poincaré plot analysis (SPPA); (left) standard Poincaré plot with $SD1$ and $SD2$; (middle) the rotated Poincaré plot (45 degrees) and (right) the segmented Poincaré plot for SPPA. (BBI = beat-to-beat intervals; \tilde{BBI} = transformed BBI after segmentation; $SD1$ = minor axis of the cloud (short-term variability); $SD2$ = major axis of the cloud (long-term variability))

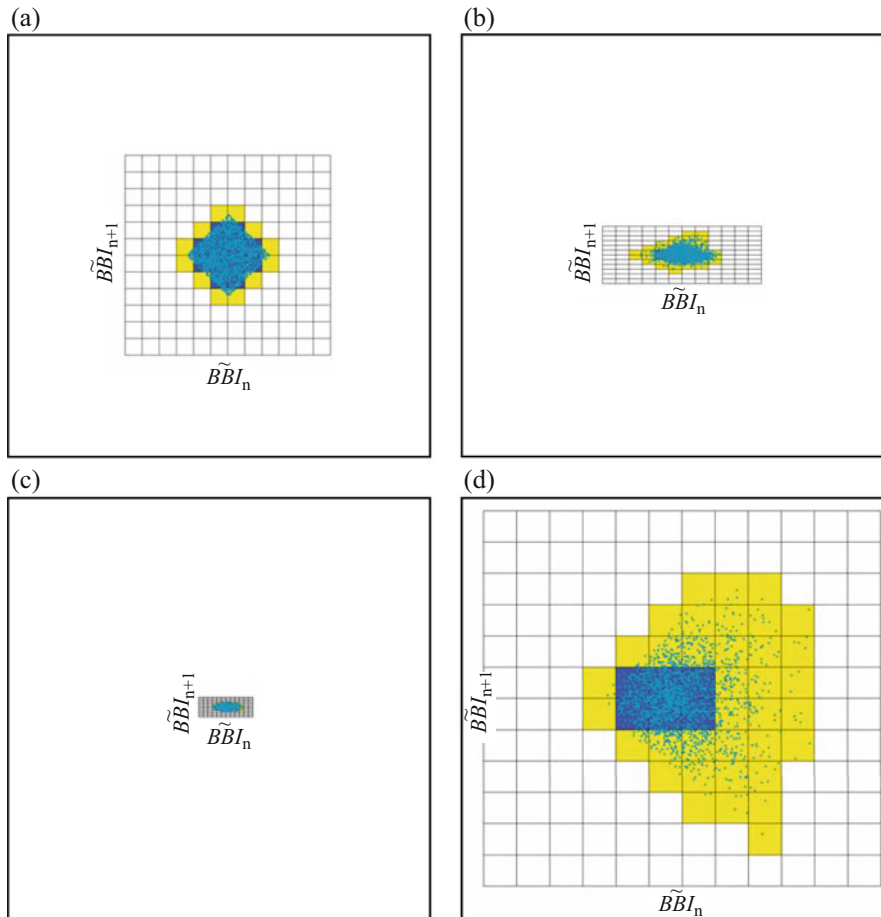


Fig. 2.7 Segmented Poincaré plot analysis: Segmented Poincaré plots of BBI time series of (a) white noise, (b) a healthy subject, (c) a patient suffering from coronary heart disease and (d) a patient suffering from atrial fibrillation. (BBI = beat-to-beat intervals)

Additionally, the Shannon entropy [bit] of the 12×12 probability matrix quantifying its disorder or uncertainty will be estimated.

An example of segmented Poincaré plots obtained from BBI time series of white noise, a healthy subject, a patient suffering from coronary heart disease and a patient suffering from atrial fibrillation are shown in Fig. 2.7.

2.2.2.2 Bivariate Segmented Poincaré Plot Analysis – (2DSPPA)

2DSPPA [90] based on the univariate SPPA [26] and works in the way that BBI time series were plotted over systolic or diastolic blood pressure (SYS, DIA) NN

time series. In this study, the interactions between BBI and SYS, BBI and DIA as well as between SYS and DIA were investigated. Based upon the single probabilities (see SPPA), all row (i) and column (j) probabilities were calculated by summation of the related single probabilities:

- 2DSPPA_r_i = single probability of each row with $i = 1-12$,
(e.g. BBI-SYS_r_1 = the single probability of the BBI time series plotted over the systolic blood pressure (SYS) NN time series in row 1)
- 2DSPPA_c_j = single probability of each column with $j = 1-12$.

2.2.2.3 Trivariate Segmented Poincaré Plot Analysis – (3DSPPA)

Three-dimensional SPPA (3DSPPA) uses three shifted signals from a time series (univariate) or three different signals (multivariate: e.g. BBI, SBP, DIA and RESP) plotted in several box models. 3DSPPA based on specific subdivisions of a cubic box model which is similar to SPPA [16, 91] and is able to investigate multivariate couplings between subsystems, e.g. of cardiovascular and cardiorespiratory autonomic regulation. Thereby, the 3DSPPA considers two varying positions of the cloud of points:

- Non-rotated version
- Rotated version [91].

According to the size of the boxes within the 3D cubes plot the cubic box model is subdivided into $12 \times 12 \times 12$ equal dimensioned cubelets for a total number of $N = 1728$ cubelets. In addition, 3DSPPA considers two approaches differing in the dimension of the cubelets calculated for both the rotated and non-rotated position of the cloud of points:

- Adapted 3DSPPA (calculation of the standard deviations $SD1$ and $SD2$ of the time series; cubelet size is adapted to the calculated SD with regard to the axis; 3D cubic box model consists of $12 \times 12 \times 12$ equal cubelets whereby the center of the cubic box represents the main focus of the cloud of points)
- Predefined 3DSPPA (3D cubic box model represents the basic model with regard to all investigated subjects).

In accordance to SPPA for each cubelet the probability of occurrence ($p_{r,c,d}$) of data points within the cubelet is calculated where the indices r represents the row, c the column and d the depth of the specific cubelet (1–12) [16, 91].

2.2.2.4 Lagged Segmented Poincaré Plot Analysis – (LSPPA)

The SPPA does not provide information about physiological changes, and especially, their relation to frequency bands corresponding to high-frequency (HF), low-frequency (LF) and very low-frequency (VLF) bands. To overcome this limitation,

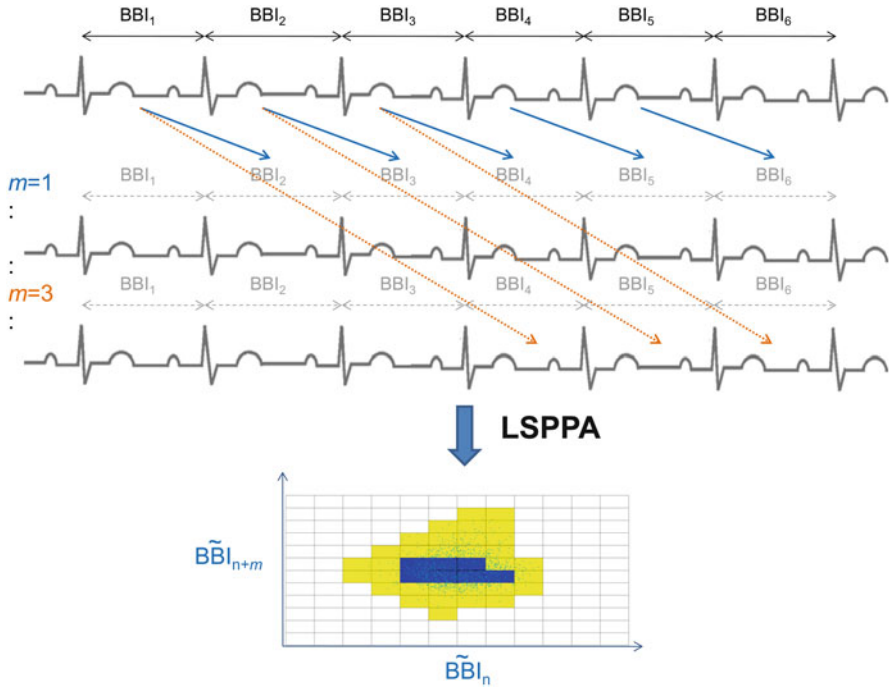


Fig. 2.8 Basic principal of time correlation analysis applying lagged segmented Poincaré plot analysis (LSPPA) for BBI time series (lags: $m = 1, m = 3$). (BBI = beat-to-beat intervals; \tilde{BBI} = transformed BBI after segmentation)

the lagged segmented Poincaré plot analysis (LPPA) was introduced (Fig. 2.8) [27]. LSPPA based on SPPA considering NN_n as a function of its subsequent NN_{n+m} by a lag of one ($m = 1$). Thereby, the lag is defined as the distance between the investigated NN . Assuming that LSPPA can describe time correlations, we have investigated the patterns of LSPPA, applying lags from $m = 1$ –100. To make the calculated results comparable, we used the same time series length for each lag by cutting an offset (specific number of NN ; $offset = 100 - m$) at the end of each time series leading to:

$$NN_n = (NN_1, NN_2, \dots, NN_{N-m-offset})$$

and

$$NN_{n+m} = (NN_2, NN_3, \dots, NN_{N-offset})$$

For each lag, the normalized probability of point occurrence in rows and columns related to the 12×12 rectangle grid is evaluated. According to SPPA, the size

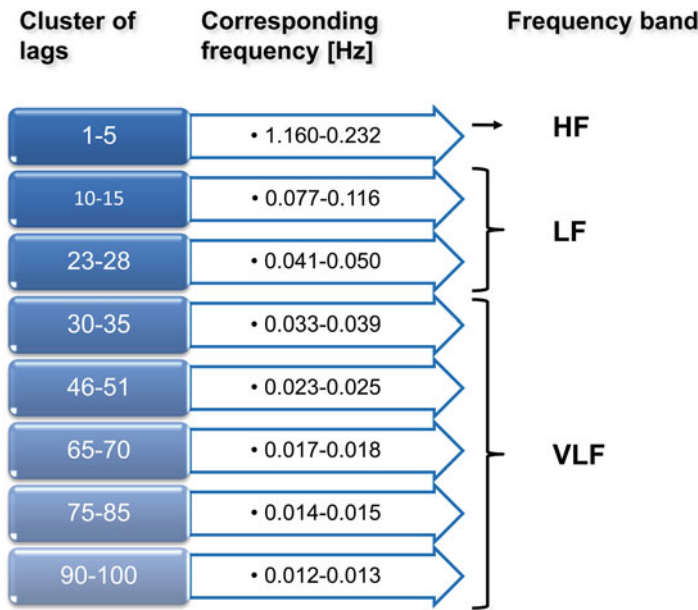


Fig. 2.9 Declaration of clusters of lags including their corresponding frequencies and the related frequency bands for lagged segmented Poincaré plot analysis

of the rectangles is adapted on *SD1* and *SD2* and depends on *m* in the lagged version of SPPA where the corresponding frequency *f* is calculated as follows: $f = 1/m * meanNN$. For a mean heart rate of 60 beats/min (*meanNN* = 1000 msec) the lowest frequency resolution will be 0.01 Hz. Afterwards, the lags are combined into eight different clusters covering the most significant frequencies (Fig. 2.9). The defined clusters include 5–11 lags independently to usually considered frequency bands. Each cluster consists of at least 75% lags with highly significant indices. Lower clusters include 5–6 lags, whereas the upper ones include 10–11 lags, according to the degree of differences between the related frequencies [27, 91].

The clusters correspond to the standardized frequency bands as HF-band (0.15–0.4 Hz) corresponds to cluster I, LF-band (0.04–0.15 Hz) corresponds to (clusters II and III), and VLF-band (0.003–0.04 Hz) corresponds to (clusters IV–VIII). Thus, LSPPA is able to provide additional information about various oscillations of the underlying physiological mechanisms of autonomic regulation as respiratory (0.145–0.6 Hz), intrinsic myogenic (0.052–0.145 Hz), neurogenic/sympathetic (0.021–0.052 Hz) and endothelial (0.0095–0.021 Hz) activities [27] (Fig. 2.9).

2.2.2.5 Complex Correlation Measure – (CCM)

Karmakar et al. [92] introduced the Complex Correlation Measure (CCM) quantifying temporal aspect of the Poincaré plot and is a function of multiple lag correlation of a investigated time series and incorporating point-to-point variation of the signal in contrast to the standard *SD1* and *SD2* PPA indices.

CCM is computed in a windowed manner embedding the temporal information of the investigated time series. Here, a moving window of three consecutive points from the Poincaré plot is considered and the area of the triangle formed by these three points is computed that measures the temporal variation of the points in the window. If three points are aligned on a line then the area is zero, which represents the linear alignment of the points. Moreover, since the individual measure involves three points of the two dimensional plot, it is comprised of at least four different points of the time series for lag $m = 1$ and at most six points in case of lag $m \geq 3$. Hence the measure conveys information about four different lag correlation of the signal. [16, 92] CCM may be used to study the lag response behavior of any pathological condition in comparison with normal subjects [16].

2.2.2.6 Specifics and Restrictions

PPA /SPPA/LSPPA: *SD1* and *SD2* dependent on other time-domain measures; short- and long term time series analyses; identifies outlier (ectopic beat or artefact); multi-lagged Poincaré plot analyses provide more information than any measure from single lagged Poincaré plot analyses [93]; different lag plots (e.g. $m = 3$) better reveal the behavior of the signal than the single lag plot; Poincaré plot at any lag m is more of a generalized scenario, where other levels of temporal variation of the dynamic system are hidden [16]; SPPA retains nonlinear features of the investigated time series, therefore overcoming some limitations of traditional PPA.

CCM is not only related to the *SD1* and *SD2*, but it also provides temporal information, which can be used to quantify the temporal dynamics of the system [16].

2.2.3 Compression Entropy

An approach to describe the entropy of a text was introduced in the framework of algorithmic information theory. Here, the entropy (Kolmogorov-Chaitin complexity) of a given text is defined as the smallest algorithm that is capable of generating the text [94]. Although it is theoretically impossible to develop such an algorithm data compression techniques might be a sufficient approximation. Ziv and Lempel [36] introduced in 1977 an universal algorithm for lossless data compression (LZ77) using string-matching on a sliding window. Today, this algorithm is widely used and implemented in compression utilities such as GIF image compression and

WinZip®. The algorithm is briefly described here that a sequence $x = x_1, x_2, \dots, x_n$ of symbols of length L of a given alphabet Θ of size $\Phi = |\Theta|$ has to be compressed. Subsequences x_m, x_{m+1}, \dots, x_n of x will be denoted as x_m^n . The algorithm keeps the most w recently encoded symbols in a sliding window. The not-yet-encoded sequence of symbols is stored in the look-ahead buffer of size b . The compressor positioned at p the first string in the look-ahead buffer looks for the longest string match of length n between the not-yet-encoded string and the strings x_p^{p+n-1} and the already-coded string in the sliding window $x_{p-w+v}^{p-w+v+n-1}$ beginning at position v . Therefore, the matching string is fully described by n and v . In short, the LZ77 algorithm operates in the following steps:

1. Encode the first w symbols without compression,
2. Set the pointer $p = w + 1$,
3. Find for some v in the range of $1 \leq v \leq w$ the largest n in the range of $1 \leq n \leq b$ such that $x_p^{p+n-1} = x_{p-w+v}^{p-w+v+n-1}$.
4. Encode the integers n and v into unary-binary code and the symbol $x_{p+n} \in \Theta$ without compression,
5. Set the pointer p to $p = n + 1$ and go to step 3 (iterate).

Assuming that the source is an ergodic process and the length of the compressed text is large ($L \rightarrow \infty$) the entropy of the compressed string H_c is determined as the length M of the compressed string divided by the length L of the original data series [37, 95].

$$H_c = M/L$$

This algorithm can be applied in a modified way for analysis of heart beat time series [37]. Here, the compression entropy H_c of heart beat time series is affected by the sample rate s , the window length w and the look-ahead buffer size b and hence denoted as $H_c^{s,w,b}$. In summary, $H_c^{s,w,b}$ indicates in which extent data from heart beat time series or each other time series can be compressed using the detection of repetitive sequences. H_c decreases with increasing window length w but the influence of the look-ahead buffer size b on H_c is only marginal. The parameters w and buffer b were optimized to $H_c^{7,3}$ ($w = 7, b = 3$) [96]. The dependency of $H_c^{s,w,b}$ on w and b suggests a sensitive of $H_c^{s,w,b}$ to vagally rather than sympathetically mediated components of HRV. Assuming that the compressibility of a time series is a measure of its nonlinear complexity, the complexity of heart rate in high-risk patients is reduced and, therefore, compression entropy decreases with increasing risk [96].

Examples of compression entropy (compressibility) obtained from BBI time series of white noise, a healthy subject, a patient suffering from coronary heart disease and a patient suffering from atrial fibrillation are shown in Fig. 2.10.

2013, Baumert et al. [35] investigated the compressibility of heart rate time series on multiple time scales, using a coarse-graining procedure applying the H_c algorithm ten times. Thereby, scale one corresponds to the original time series, higher scales (2–10) were obtained by coarse-graining procedure, using the procedure proposed by Costa et al. [97] multiscale entropy algorithm. Here, an one-dimensional discrete time series, $\{x_1, \dots, x_i, \dots, x_N\}$, the coarse-grained

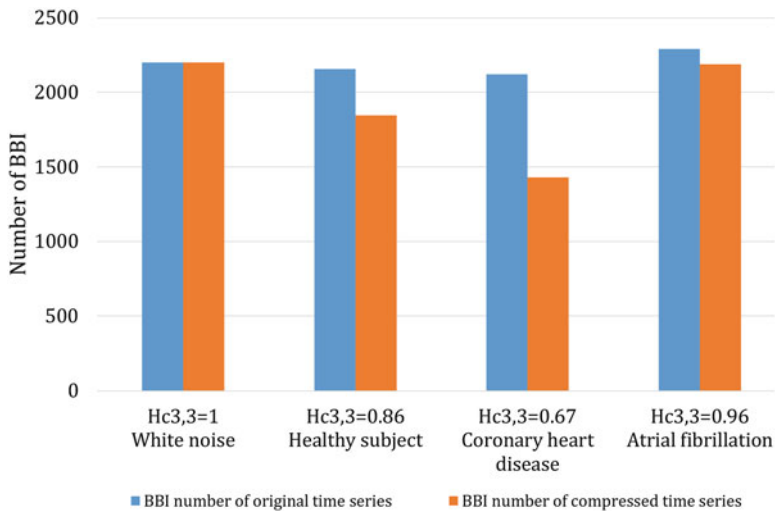


Fig. 2.10 Compression entropy: Compressibility (window length, $w = 3$, buffer length, $b = 3$) for BBI time series. Illustrative comparison of the length of the original (blue) vs. compressed (orange) BBI time series of white noise, healthy subjects, patients suffering from coronary heart disease and atrial fibrillation. (BBI = beat-to-beat intervals)

time series $\{x(\tau)\}$ determined by the scale factor τ is constructed by $x_j^{(\tau)} = 1/\tau \sum_{i=(j-1)\tau+1}^{j\tau} x_i$ where τ represents the scale factor and $1 \leq j \leq L/\tau$. In other words, coarse-grained time series for scale τ were obtained by taking arithmetic mean of τ neighboring original values without overlapping. For scale 1, the coarse grained time series is simply the original time series. They concluded that multiscale investigation of compressibility may provide an alternative method for entropy assessment of biomedical signals over different time scales and be particularly useful for heart rate complexity analysis.

A limitation of all univariate methods is that they are not able to quantify the direct interrelationships between different time series. Therefore, they have limited power to reveal the underlying physiological mechanisms responsible for changes in time series complexity.

Recently, Li and Vitányi [94] compared several entropy and entropy rate based methods. They investigated the hypothesis that the linear model-based (MB) approach for the estimation of conditional entropy (CE) can be utilized to assess the complexity of the cardiac control in healthy individuals in comparison to nonlinear model-free (MF) methods such as corrected ApEn, SampEn, corrected CE, two k-nearest-neighbor CE procedures and permutation CE. They found, that the MB approach can be utilized to monitor the changes of the complexity of the cardiac control, thus speeding up dramatically the CE calculation. They concluded that, due to that the remarkable performance of the MB approach challenges the notion, generally assumed in cardiac control complexity analysis based on CE, about the need of MF techniques and could allow real time applications.

2017, Schumann et al. [98] introduced the cross-compression entropy (CH_c). CH_c combines the data compression technique based on symbol transformation and the principle of causality. It estimates to which extent a time series (target) can be compressed by another (source) beyond its own past. The improvement of compression considering the source signal is equivalent to an increase of predictability of the target's future. Therefore, CH_c represents a measure of causality between coarse-grained time series in compliance with the notion of Wiener and Granger [99]. First, the input time series are transformed into sequences of symbols [77]. In analogy to the univariate compression procedure, a memory window and a buffer window are shifted along the target series [37, 96]. Additionally, a memory window is defined in the source series that is used to encode the target symbols. The target buffer window covers B_y symbols $Y_p^{p+B_y}$, starting at the current data point Y_p (coding position). These target symbols are encoded using the symbols of the source memory window $X_{p-M_x}^{p-1}$ with length M_x . The longest subseries $X_{p-M_x+v-1}^{p-M_x+v+n-2}$, lasting n source symbols starting at element v , that matches the target sequence Y_p^{p+n-1} is extracted. Instead of encoding the whole target string, the starting point v and the length n of its equivalent in the source memory and the successor X_{p+n} is stored. Hence, n target symbols can be passed and the new coding position is X_{p+n+1} .

If there is a redundant substring, of the same length or longer, included in the target memory, compressibility is not improved by taking the source signal into account. Therefor matching source symbols are ignored, if a substring $Y_{p-M_y+k-1}^{p-M_y+k+l-2}$ with a length of $l \geq n$ in the target memory matches Y_p^{p+l-1} .

$\text{CH}_{cX \rightarrow Y}$ is defined as the proportion of iterations that can be saved compressing Y_i by X_i with respect to the original length of Y_i . Assuming the input Y_i of length N_0 is compressed by X_i in N_{com} iterations, CH_c is calculated by the equation below.

$$\text{CH}_{cX \rightarrow Y} = \frac{N_0 - N_{com}}{N_0}$$

Because redundant symbol patterns at different positions in the source window (start v) can contribute to the compression, CH_c allows the delay of coupling to vary during the time of acquisition. The interaction across various time scales can be covered by CH_c due to a variable length of redundant symbol substrings n . Although CH_c is very flexible, it is easy to interpret and has the natural boundaries of zero and one. The compression algorithm is well known and easy to implement. Symbolization is robust to outliers and does not require stationarity of the data.

2.2.3.1 Specifics and Restrictions

Dependency on sampling rate, the window length, the look-ahead buffer size and a threshold; implementation has to consider integer numbers; relatively insensitive to

artefacts and non-stationarity which have only a locally limited influence; short-term method where longer lasting patterns reflecting especially sympathetically mediated influences are not or only partially considered for compression; short- and long term time series analyses.

2.3 Clinical Applications

2.3.1 *Schizophrenia: Cardiorespiratory System*

Schizophrenia is a severe mental disorder associated with a significantly increased cardiovascular mortality rate. However, the underlying mechanisms leading to cardiovascular disease (CVD) are not fully known. For the quantitative analyses of the cardiorespiratory system in univariate and bivariate ways, several linear and nonlinear time series analysis approaches were developed. Studies indeed showed that the coupling between the cardiovascular system and respiration is strongly nonlinear [100]. Therefore, linear methods seem to be inappropriate and not able to fully address physiological regulatory mechanisms within the cardiovascular system. Methods based on entropies have the common feature that they analyze a putative information transfer between time series and address either the uncertainty or predictability of time series. Complexity analysis can be performed by evaluating the entropy and entropy rate. Entropy (e.g., Shannon or Renyi) calculates the degree of complexity of a signal's sample distribution. However, a limitation of all univariate nonlinear methods is that they are not able to quantify the direct interrelationships such as the nonlinear influence of respiration on heart rate. Therefore, they have limited power to reveal the underlying physiological mechanisms responsible for changes in cardiorespiratory complexity [76].

We investigated [76, 101, 102] non-medicated 23 patients with schizophrenia (SZ; 12 male; 30.4 ± 10.3 years) and 23 healthy subjects (CO, 13 male; 30.3 ± 9.5 years) matched regarding to age and sex (Table 2.1) to quantify heart rate- and respiratory variability (HRV, RESPV) and their dynamics as well as the cardiorespiratory coupling (CRC).

Patients were included only when they had not taken any medication for at least 8 weeks. Diagnosis of paranoid schizophrenia was established when patients fulfilled DSM-IV criteria (Diagnostic and statistical manual of mental disorders, 4th edition). Psychotic symptoms were quantified using the Positive and Negative Syndrome Scale (PANSS). A careful interview and clinical investigation was performed for all controls to exclude any potential psychiatric or other disease as well as interfering medication. The Structured Clinical Interview SCID II and a personality inventory (Freiburger Persönlichkeitsinventar, FPI) were additionally applied for controls to detect personality traits or disorders which might influence autonomic function. This study complied with the Declaration of Helsinki. All participants gave written informed consent to a protocol approved by the local Ethics

Table 2.1 Clinical and demographic data of enrolled study participants

Data	Healthy subjects	Schizophrenic patients
	(CO)x	(SZ)
Number of participants	23	23
Gender (male/female)	13/10	12/11
Age (mean \pm std. in years)	30.3 \pm 9.5	30.4 \pm 10.3
PANSS, mean (min-max)	n.a.	85.7 (43–124)
SANS, mean (min-max)	n.a.	49.6 (14–81)
SAPS, mean (min-max)	n.a.	60.9 (6–108)

Psychotic symptoms for acute schizophrenia were quantified using the scale for the assessment of positive symptoms (SAPS) and negative symptoms (SANS) and positive and negative syndrome scales (PANSS); n.A. means not applicable

Committee of the University Hospital Jena. Patients were advised that the refusal of participating in this study would not affect future treatment.

From all subjects a high resolution short-term ECG (1000 Hz sampling frequency) and synchronized calibrated respiratory inductive plethysmography signal (LifeShirt[®], Vivometrics, Inc., Ventura, CA, U.S.A.) were recorded for 30 min. Investigations were performed between 3 and 6 p.m. in a quiet room which was kept comfortably warm (22–24 °C) and began after subjects had rested in supine position for 10 min. Subjects were asked to relax and to breathe normally to avoid hyperventilation. No further instruction for breathing was given. Subjects were asked explicit not to talk during the recording. Following time series were automatically extracted from the raw data records as:

- Time series of heart rate consisting of successive beat-to-beat intervals (BBI) and
- Time series of respiratory frequency (RESP) as the time intervals between consecutive breathing cycles.

Quantification of HRV, RESPV and CRC was done by applying several complexity approaches as symbolic dynamics (SD), compression entropy (H_C), sample entropy (SampEn), Poincaré plot analysis (PPA), Higuchi fractal dimension (HD), high resolution joint symbolic dynamics (HRJSD), cross conditional entropy (CCE), cross multiscale entropy (CMSE) and normalized short time partial directed coherence (NSTPDC) [71, 76, 103].

The nonparametric exact two-tailed Mann-Whitney U-test (SPSS 21.0) was performed to non-normally distributed indices (significant Kolmogorov-Smirnov test) to evaluate continuous baseline variables as well as differences in autonomic indices between SZ and CO. The significance level was set to $**p < 0.01$ (Bonferroni-Holm adjustment: $***p < 0.001$). In addition, all results were presented as mean \pm standard deviation.

We found (Table 2.2, Figs. 2.11, 2.12, and 2.13) significant difference in HRV, RESPV and their dynamics as well as in CRC in SZ in comparison to CO ($p < 0.001$). Especially, we demonstrated by different complexity based measures (univariate, bivariate) that HRV was characterized by reduced complexity

Table 2.2 Univariate statistical analysis results of heart rate- and respiratory variability in the complexity domain to discriminate between patients suffering from schizophrenia (SZ) and healthy subjects (CO)

	Index	p	CON	SZ
			Mean \pm Std	Mean \pm Std
SD	SD _{Renyi025_BBI}	**	3.74 \pm 0.37	3.47 \pm 0.37
	Forbword _{BBI}	**	15.04 \pm 13.25	25.91 \pm 12.35
	SD _{Renyi025_RESP}	***	3.23 \pm 0.15	3.47 \pm 0.19
	Forbword _{RESP}	**	31.61 \pm 4.53	23.65 \pm 6.41
H _C	H _{C_BBI}	***	0.82 \pm 0.10	0.69 \pm 0.10
	H _{C_RESP}	n.s.	0.59 \pm 0.08	0.59 \pm 0.12
SampEn	SampEn _{BBI}	**	2.29 \pm 0.30	1.96 \pm 0.47
	SampEn _{RESP}	n.s.	1.32 \pm 0.37	1.49 \pm 0.50
PPA	SD1/SD2 _{BBI}	***	0.46 \pm 0.16	0.29 \pm 0.11
	SD1/SD2 _{RESP}	***	0.11 \pm 0.03	0.18 \pm 0.06
HD	HD _{RSA}	**	1.14 \pm 0.03	1.19 \pm 0.05
HRJSD	HRJSD _{Renyi025}	***	4.06 \pm 0.11	4.37 \pm 0.15
CCE	CCE _{uf_BBI-RESP}	**	0.12 \pm 0.07	0.16 \pm 0.08
CMSE	CMSE _{scale1}	***	2.13 \pm 0.67	1.43 \pm 0.42
NSTPDC	H _{BBI→RESP}	**	0.78 \pm 0.07	0.71 \pm 0.09
	H _{RESP→BBI}	***	0.76 \pm 0.05	0.71 \pm 0.05

BBI beat-to-beat intervals, *RESP* time intervals between consecutive breathing cycles, *SD* symbolic dynamics, *H_C* compression entropy, *SampEn* sample entropy, *PPA* Poincaré plot analysis, *HD* Higuchi fractal dimension (*RSA* respiratory sinus arrhythmia), *HRJSD* high resolution joint symbolic dynamics, *CCE* cross conditional entropy, *CMSE* cross multiscale entropy; *NSTPDC* normalized short time partial directed coherence, mean value \pm standard deviation, *p* univariate significance (***p* < 0.01, ****p* < 0.001, *n.s.* not significant)

(Figs. 2.11, and 2.12), whereas RESPV was characterized by increased complexity and CRC was reduced accompanied by reduced complexity in schizophrenia.

These results suggest a parasympathetic withdrawal and an ongoing sympathetic predominant activation in cardiac autonomic regulation. Bär et al. [43] suggested that the reduction in heart rate complexity indicates that heart rate cannot adapt to different requirements arising from posture or exertion and that the heart is at higher risk of developing arrhythmias in those patients. Voss et al. [104] found also reduced HRV (linear, nonlinear) in schizophrenic patients and their relatives, indicating an impaired autonomic function, widely believed to be caused by a reduced vagal tone. They further stated that at this moment the association of a reduced HRV and higher cardiac risk (high mortality rates) for those patients has not been satisfactorily proven. In general, the reduction in cardiac complexity supports the thesis of a changed sympathetic/parasympathetic heart rate control in schizophrenic patients [1]. A reduction of cardiac complexity (the increase of cardiac regularity) is considered as a marker of pathology.

Considering respiration and respiratory variability (Fig. 2.13) as well as their complexity we found, in accordance to previous findings [102, 105, 106]. Homma

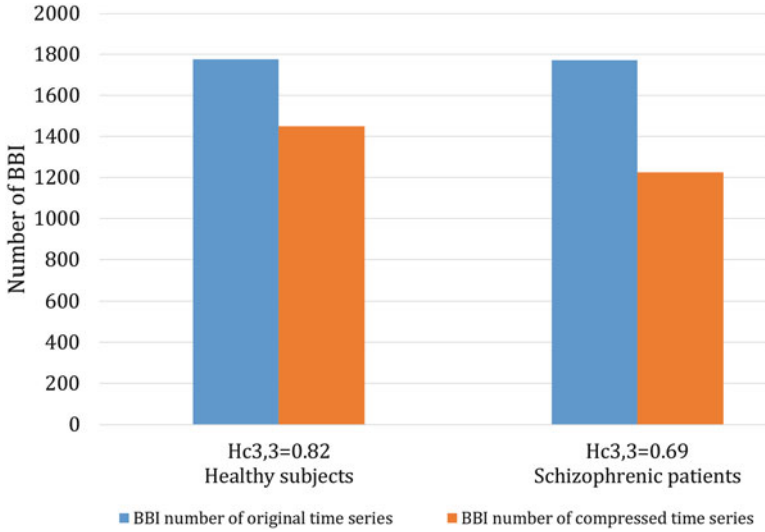


Fig. 2.11 Compression entropy: Compressibility (window length, $w = 3$, buffer length, $b = 3$) for BBI time series. Illustrative comparison of the length of the original (blue) vs. compressed (orange) BBI time series for patients suffering from (right) schizophrenia ($H_{c,3}^{3,3} = 0.69$) and (left) healthy subjects ($H_{c,3}^{3,3} = 0.82$). (BBI = beat-to-beat intervals)

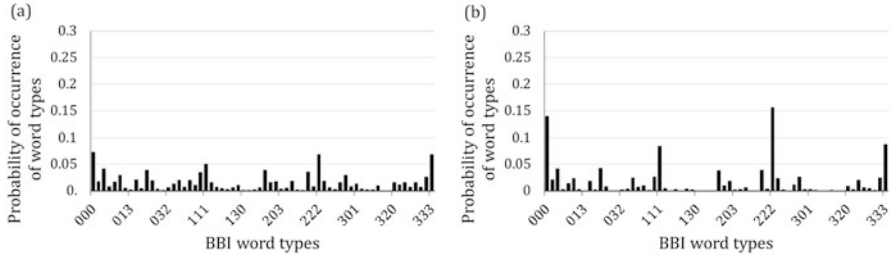


Fig. 2.12 Symbolic dynamics: Word distributions (histograms) obtained from BBI time series applying symbolic dynamic analysis of (a) healthy subjects and (b) patients suffering from schizophrenia. (BBI = beat-to-beat intervals)

et al. [107] stated that the final respiratory output involves a complex interaction between the brainstem and higher centers, including the limbic system and cortical structures. Respiration is primarily regulated for metabolic and homeostatic purposes in the brainstem and also changes in response to changes in emotions, such as sadness, happiness, anxiety or fear. Williams et al. [108] could show a functional disconnection in autonomic and central systems for processing threat-related signals in patients with paranoid schizophrenia and hypothesized that paranoid cognition may reflect an internally generated cycle of misattribution regarding incoming fear

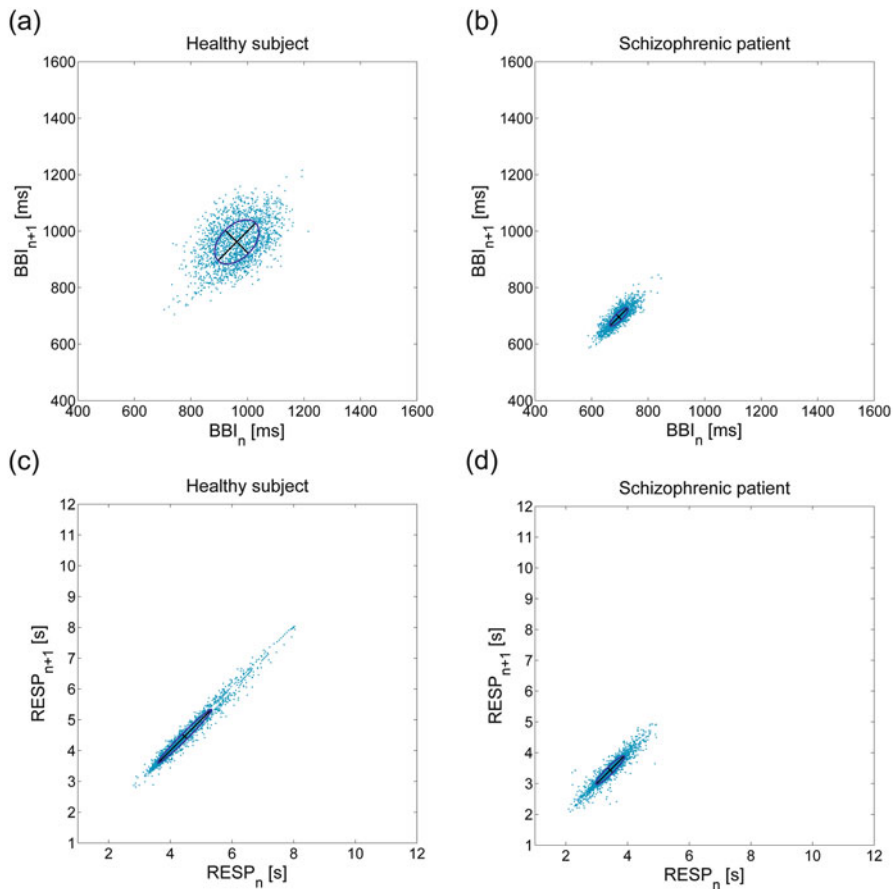


Fig. 2.13 Poincaré plot analysis: Standard Poincaré plots of BBI time series of (a) a healthy subject and (b) a patient suffering from schizophrenia, and of respiratory frequency intervals (RESP) of (c) a healthy subject and (d) a patient suffering from schizophrenia. (BBI = beat-to-beat intervals; RESP = respiratory frequency)

signals due to a breakdown in the regulation of these systems. Boiten et al. [109] found that respiration patterns reflect the general dimensions of emotional response that are linked to response requirements of the emotional situations. Furthermore, the ratio of inspiration time to expiration time is closely related to emotions, but however, are inconsistent discussed [109]. The found alterations in RESPV likely can be explained that a dysregulation of arousal, as suggested in paranoid schizophrenia in amygdalae prefrontal circuits, might contribute to the correlation of psychopathology and breathing alterations [102]. In contrast to HRV respiration was characterized by increased entropy indices ($SD_{Renyi025_RESP}$, $SampEn_RESP$, and $HDRSA$) indicating that fractal characteristics (morphological structure) of the RSA

signal were increased in SZ indicating that the underlying rhythm of the RSA signal is randomly fluctuating. These findings pointing to increased irregularity of respiration. It could be shown that a small change in respiratory functioning may lead to background symptoms of panic and anxiety in any disorder as a results of the link between the central nervous system and respiration [110]. It is well proven that schizophrenia is related to panic attacks [111, 112], further supporting the altered CRC in SZ might be at least partly related to panic attacks in the acute psychotic state. It was shown that changed complexity indices, resulting from depressed organ function, a loss of interaction among subsystems, an overwhelming action of a subsystem over others and an impairment of regulatory processes, is a clear hallmark of a pathological situation [113]. We believe that the found alterations in CRC might reflect arousal and permeant stress situation in acutely ill SZ patients. This can be confirmed by comparable physiological changes within the cardiorespiratory system in healthy subjects during stress conditions [102].

In conclusion, we showed that complexity indices from HRV; RESPV and CRC analyses could contribute to enhanced risk stratification in schizophrenic patients and possible will identify in the near future those patients at higher risk cardiovascular disease. At the moment we are just at the beginning to understand the interrelationship between the cardiorespiratory system in psychotic states and the related brainstem neural networks and control mechanisms.

2.3.2 Schizophrenia: Blood Flow

We investigated the impairment of microcirculation in schizophrenic patients by means of spectral analysis of blood flow signals and to determine if microcirculation is unequally altered in different tissue depths. Furthermore, the impact of gender and age on the spectral parameters of the Laser Doppler Flowmetry (LDF) signal in healthy and diseased microcirculation were analyzed. The Segmented Spectral Analysis (SSA) algorithm was applied to LDF signals of a provoked post-ischemic stage and compared to the traditional total spectral analysis (TSA). 15 healthy subjects (CON, mean age 32.4 years) and 15 patients (PAT, mean age 33.0 years) were enrolled. Spectral analysis was performed on two LDF signals at a depth of 2 mm and 6–8 mm. Features in five frequency subintervals were determined. Our results indicate that microcirculation is strongly impaired in patients. SSA of blood flow revealed differences between CON and PAT in all three frequency intervals referring to local vasomotion (endothelial $p = 0.03$; sympathetic $p = 0.02$, myogenic $p = 0.03$) as well as the respiratory ($p = 0.02$) and cardiac ($p = 0.006$) bands in the deeper tissue. In contrast, in the near-surface tissue only the endothelial ($p = 0.006$) and cardiac ($p = 0.006$) components were altered. Furthermore, SSA determined a gender- and age dependency regarding blood flow. In conclusion, we could demonstrate that microcirculation in schizophrenic patients is significantly impaired and that blood flow in the near-surface skin and in the superficial muscle tissue is affected differently, depending on its location in the near-surface skin

or in the superficial muscle tissue. These alterations of microcirculation are more pronounced in the deeper tissue depth of about 6–8 mm and are influenced by gender and age. [114].

2.3.3 *Idiopathic Dilated Cardiomyopathy*

Identifying idiopathic dilated cardiomyopathy (IDC) patients who are at risk of sudden death is still unsolved. The presence of autonomic imbalance in patients with IDC might predict sudden death and tachyarrhythmic events. The aim of this study was to analyze the suitability of blood pressure variability (BPV) compared to heart rate variability (HRV) for non-invasive risk stratification in IDC patients. Therefore, continuous non-invasive blood pressure and high-resolution electrocardiogram were recorded from 91 IDC patients for 30 min. During a median follow-up period of 28 months (range: [17–38] months), 14 patients died due to sudden death or necessary resuscitation due to a life-threatening arrhythmia. HRV and BPV analyses were performed in time domain, frequency domain, and nonlinear dynamics. We found that dynamics of blood pressure regulation was significantly changed in high-risk patients, indicating an increased BPV. BPV indexes from nonlinear symbolic dynamics revealed significant univariate (sensitivity: 85.7%; specificity 77.9%; area under receiver-operator characteristics [ROC] curve: 87.8%) differences. In an optimum multivariate set consisting of two clinical indexes (left ventricular end-diastolic diameter, New York Heart Association) and one nonlinear index (symbolic dynamics), highly significant differences between low- and high-risk IDC groups were estimated (sensitivity of 92.9%, specificity of 86.5%, and area under ROC curve of 95.3%). In sum, diastolic BPV indexes, especially those from symbolic dynamics, appear to be useful for risk stratification of sudden death in patients with IDC. [115].

2.3.4 *Depression*

Due to that major depressive disorders (MDD) are associated with an increased risk for cardiovascular morbidity and mortality and it is known that MDD are accompanied with an autonomic dysfunction with increased sympathetic and/or reduced parasympathetic activity to data only limited information are available about the degree and complexity of cardiovascular regulation. We investigated 57 non-medicated depressed patients in comparison to 57 healthy subjects matched with respect to age, gender and group size and the influence of MDD on autonomous nervous system by means of linear and nonlinear indices from heart rate- and blood pressure variability (HRV, BPV). Complexity indices from nonlinear dynamics demonstrated considerable changes in autonomous regulation due to MDD. For the first time we could show that non-medicated depressed patients who were matched

with respect to age, gender and group size reveal a significant changed short-term as well as long-term complexity of cardiovascular regulation. Complexity indices from nonlinear dynamics showed considerable changes in autonomous regulation caused by the disease depression. This finding was supported by linear indices only from BPV. These results suggest substantial changes in autonomic control probably due to a change of interactions between different physiological control loops in MDD. [44].

2.3.5 *Pregnancy*

Hypertensive pregnancy disorders affect 6–8% of gestations representing the most common complication of pregnancy for both mother and fetus. In this study, 10 healthy non-pregnant women, 66 healthy pregnant women and 56 hypertensive pregnant women (chronic hypertension, pregnancy induced hypertension and PE) were investigated applying the three-dimensional segmented Poincaré plot analyses (3DSPPA) to detect hypertensive pregnancy disorders and especially pre-eclampsia (PE). From all subjects 30 min of beat-to-beat intervals (BBI), respiration (RESP), non-invasive systolic (SBP) and diastolic blood pressure (DBP) were continuously recorded and analyzed. Non-rotated adapted 3DSPPA discriminated best between hypertensive pregnancy disorders and PE concerning coupling analysis of 2 or 3 different systems (BBI, DBP, RESP and BBI, SBP, DBP) reaching an accuracy of up to 82.9%. This could be increased to an accuracy of up to 91.2% applying multivariate analysis differentiating between all pregnant women and PE. In conclusion, 3DSPPA could be a useful method for enhanced risk stratification in pregnant women [91].

2.4 Conclusion

It becomes apparent that cardiovascular regulation is one of the most complex systems in human due to the fact, that a variety of factors influencing the cardiovascular system (e.g. heart rate) [103]. The application of nonlinear dynamics is motivated by the fact that the control systems of the cardiovascular system have been shown to be nonlinear because of its high complexity and the nonlinear interactions between the physiological subsystems [103, 116]. Several of nonlinear indices have been proven to be of diagnostic relevance or have contributed to risk stratification. In this chapter we focused on the nonlinear methods symbolic dynamics, Poincaré plot analysis, and compression entropy and their recent enhanced versions. The introduced complexity methods revealed new insights into the changed autonomic nervous system under various physiological and pathophysiological conditions, provide additional prognostic information and definitely complement traditional

time and frequency domain analyze. These methods have already been proven to be of diagnostic relevance or have contributed to risk stratification in different diseases.

Several metrics assessing the system's complexity and information flow among its components are based on symbolization techniques. Indices derived from symbolic dynamics might provide a reliable alternative to markers of complexity and causality that can be derived from model-based multiple linear regression approaches in time and frequency domains [117–120]. In the medical field, it can be expected that symbolic dynamics will have a powerful impact in the coming years by playing a significant role in tailoring individual treatments, improving diagnostics and therapy, managing patient data and reducing the cost of healthcare systems via a more precise risk stratification [15].

Research on HRV has proven that Poincaré plot analysis is a powerful tool to evaluate short term and long term HRV. Researchers have investigated a number of methods: converting the two- or three-dimensional Poincaré plot into various one-dimensional views; segmented the plot to retain nonlinear properties of the underlying system; multiple lagged plot analysis to investigate time correlation of the system; the fitting of an ellipse to the plot shape; and measuring the correlation coefficient of the plot. Poincaré plot analyses play a more and more important role and—as an advantage—are easier to understand and interpret [16].

Methods based on entropies have in common that they analyze a putative information transfer within one or between time series and address the uncertainty or predictability of time series. Compression entropy represents only one complexity measure within the big group of methods calculating entropy and/or entropy rates. This method is easy to apply, working time efficiently and allows straightforward physiological interpretations.

Applications of these introduced methods in future studies are very promising and should (depending on the complexity of the investigated system) be performed in a multivariate manner complemented with linear and further successful non-linear approaches.

References

1. Voss, A., Schulz, S., Schroeder, R., Baumert, M., Caminal, P.: Methods derived from nonlinear dynamics for analysing heart rate variability. *Philos. Transact. A Math. Phys. Eng. Sci.* **367**, 277–296 (2009)
2. Porta, A., Tobaldini, E., Guzzetti, S., Furlan, R., Montano, N., Gneccchi-Ruscone, T.: Assessment of cardiac autonomic modulation during graded head-up tilt by symbolic analysis of heart rate variability. *Am. J. Physiol. Heart Circ. Physiol.* **293**, H702–H708 (2007)
3. Cysarz, D., Porta, A., Montano, N., Leeuwen, P.V., Kurths, J., Wessel, N.: Quantifying heart rate dynamics using different approaches of symbolic dynamics. *Eur. Phys. J. Spec. Top.* **222**, 487–500 (2013)
4. Baumert, M., Walther, T., Hopfe, J., Stepan, H., Faber, R., Voss, A.: Joint symbolic dynamic analysis of beat-to-beat interactions of heart rate and systolic blood pressure in normal pregnancy. *Med. Biol. Eng. Comput.* **40**, 241–245 (2002)

5. Schulz, S., Haueisen, J., Bar, K.J., Andreas, V.: High-resolution joint symbolic analysis to enhance classification of the cardiorespiratory system in patients with schizophrenia and their relatives. *Philos. Trans. A Math. Phys. Eng. Sci.* **373**, 20140098 (2015)
6. Voss, A., Kurths, J., Kleiner, H.J., Witt, A., Wessel, N., Saperin, P., et al.: The application of methods of non-linear dynamics for the improved and predictive recognition of patients threatened by sudden cardiac death. *Cardiovasc. Res.* **31**, 419–433 (1996)
7. Wackermann, J., Lehmann, D., Michel, C.M., Strik, W.K.: Adaptive segmentation of spontaneous EEG map series into spatially defined microstates. *Int. J. Psychophysiol.* **14**, 269–283 (1993)
8. Beim Graben, P., Hutt, A.: Detecting recurrence domains of dynamical systems by symbolic dynamics. *Phys. Rev. Lett.* **110**, 154101 (2013)
9. Schindler, K., Gast, H., Stieglitz, L., Stibal, A., Hauf, M., Wiest, R., et al.: Forbidden ordinal patterns of perictal intracranial EEG indicate deterministic dynamics in human epileptic seizures. *Epilepsia*. **52**, 1771–1780 (2011)
10. Hively, L.M., Protopopescu, V.A., Munro, N.B.: Enhancements in epilepsy forewarning via phase-space dissimilarity. *J. Clin. Neurophysiol.* **22**, 402–409 (2005)
11. Mashour, G.A.: Cognitive unbinding: a neuroscientific paradigm of general anesthesia and related states of unconsciousness. *Neurosci. Biobehav. Rev.* **37**, 2751–2759 (2013)
12. Staniek, M., Lehnertz, K.: Symbolic transfer entropy: inferring directionality in biosignals. *Biomed. Tech. (Berl)*. **54**, 323–328 (2009)
13. Voss, A., Schulz, S., Schroeder, R.: Monitoring in cardiovascular disease patients by nonlinear biomedical signal processing. *Conf. Proc. IEEE Eng. Med. Biol. Soc.* **2011**, 6564–6567 (2011)
14. Schulz, S., Bolz, M., Bar, K.J., Voss, A.: Central- and autonomic nervous system coupling in schizophrenia. *Philos. Trans. A Math. Phys. Eng. Sci.* **374**, 20150178 (2016)
15. Porta, A., Baumert, M., Cysarz, D., Wessel, N.: Enhancing dynamical signatures of complex systems through symbolic computation. *Philos. Trans. A Math. Phys. Eng. Sci.* **373**, 20140099 (2015)
16. Khandoker, A.H., Karmakar, C., Brennan, M., Palaniswami, M., Voss, A.: Poincaré plot methods for heart rate variability analysis. Springer, London (2013)
17. Kamen, P.W., Krum, H., Tonkin, A.M.: Poincare plot of heart rate variability allows quantitative display of parasympathetic nervous activity in humans. *Clin. Sci. (Lond.)* **91**, 201–208 (1996)
18. Weiss, J.N., Garfinkel, A., Spano, M.L., Ditto, W.L.: Chaos and chaos control in biology. *J. Clin. Invest.* **93**, 1355–1360 (1994)
19. Babloyantz, A., Destexhe, A.: Is the normal heart a periodic oscillator? *Biol. Cybern.* **58**, 203–211 (1988)
20. Woo, M.A., Stevenson, W.G., Moser, D.K., Trelease, R.B., Harper, R.M.: Patterns of beat-to-beat heart rate variability in advanced heart failure. *Am. Heart J.* **123**, 704–710 (1992)
21. Brennan, M., Palaniswami, M., Kamen, P.: Poincare plot interpretation using a physiological model of HRV based on a network of oscillators. *Am. J. Physiol. Heart Circ. Physiol.* **283**, H1873–H1886 (2002)
22. Kamen, P.W., Tonkin, A.M.: Application of the Poincare plot to heart rate variability: a new measure of functional status in heart failure. *Aust. NZ J. Med.* **25**, 18–26 (1995)
23. Laitio, T.T., Huikuri, H.V., Kentala, E.S., Makikallio, T.H., Jalonen, J.R., Helenius, H., et al.: Correlation properties and complexity of perioperative RR-interval dynamics in coronary artery bypass surgery patients. *Anesthesiology*. **93**, 69–80 (2000)
24. Kleiger, R.E., Stein, P.K., Bigger Jr., J.T.: Heart rate variability: measurement and clinical utility. *Ann. Noninvasive Electrocardiol.* **10**, 88–101 (2005)
25. Brennan, M., Palaniswami, M., Kamen, P.: Do existing measures of Poincare plot geometry reflect nonlinear features of heart rate variability? *I.E.E.E. Trans. Biomed. Eng.* **48**, 1342–1347 (2001)

26. Voss, A., Fischer, C., Schroeder, R., Figulla, H.R., Goernig, M.: Segmented Poincare plot analysis for risk stratification in patients with dilated cardiomyopathy. *Methods Inf. Med.* **49**, 511–515 (2010)
27. Voss, A., Fischer, C., Schroeder, R., Figulla, H.R., Goernig, M.: Lagged segmented Poincare plot analysis for risk stratification in patients with dilated cardiomyopathy. *Med. Biol. Eng. Comput.* **50**, 727–736 (2012)
28. Tulppo, M.P., Makikallio, T.H., Takala, T.E., Seppanen, T., Huikuri, H.V.: Quantitative beat-to-beat analysis of heart rate dynamics during exercise. *Am. J. Phys.* **271**, H244–H252 (1996)
29. Rajendra Acharya, U., Joseph, K.P., Kannathal, N., Lim, C.M., Suri, J.S.: Heart rate variability: a review. *Med. Biol. Eng. Comput.* **44**, 1031–1051 (2006)
30. Tulppo, M.P., Makikallio, T.H., Seppanen, T., Airaksinen, J.K., Huikuri, H.V.: Heart rate dynamics during accentuated sympathovagal interaction. *Am. J. Phys.* **274**, H810–H816 (1998)
31. Fischer, C., Seeck, A., Schroeder, R., Goernig, M., Schirdewan, A., Figulla, H.R., et al.: QT variability improves risk stratification in patients with dilated cardiomyopathy. *Physiol. Meas.* **36**, 699–713 (2015)
32. Stein, P.K., Reddy, A.: Non-linear heart rate variability and risk stratification in cardiovascular disease. *Ind. Pacing Electrophysiol. J.* **5**, 210–220 (2005)
33. Rydberg, A., Karlsson, M., Hornsten, R., Wiklund, U.: Can analysis of heart rate variability predict arrhythmia in children with Fontan circulation? *Pediatr. Cardiol.* **29**, 50–55 (2008)
34. Porta, A., Guzzetti, S., Montano, N., Furlan, R., Pagani, M., Malliani, A., et al.: Entropy, entropy rate, and pattern classification as tools to typify complexity in short heart period variability series. *I.E.E.E. Trans. Biomed. Eng.* **48**, 1282–1291 (Nov 2001)
35. Baumert, M., Voss, A., Javorka, M.: Compression based entropy estimation of heart rate variability on multiple time scales. *Conf. Proc. IEEE Eng. Med. Biol. Soc.* **2013**, 5037–5040 (2013)
36. Ziv, J., Lempel, A.: Universal algorithm for sequential data compression. *IEEE Trans. Inf. Ther.* **23**, 337–343 (1977)
37. Baumert, M., Baier, V., Haueisen, J., Wessel, N., Meyerfeldt, U., Schirdewan, A., et al.: Forecasting of life threatening arrhythmias using the compression entropy of heart rate. *Methods Inf. Med.* **43**, 202–206 (2004)
38. Van Leeuwen, P., Cysarz, D., Edelhauser, F., Gronemeyer, D.: Heart rate variability in the individual fetus. *Auton. Neurosci.* **178**, 24–28 (2013)
39. Boettger, M.K., Schulz, S., Berger, S., Tancer, M., Yeragani, V.K., Voss, A., et al.: Influence of age on linear and nonlinear measures of autonomic cardiovascular modulation. *Ann. Noninvasive Electrocardiol.* **15**, 165–174 (2010)
40. Voss, A., Schroeder, R., Heitmann, A., Peters, A., Perz, S.: Short-term heart rate variability—influence of gender and age in healthy subjects. *PLoS One.* **10**, e0118308 (2015)
41. Porta, A., Faes, L., Bari, V., Marchi, A., Bassani, T., Nollo, G., et al.: Effect of age on complexity and causality of the cardiovascular control: comparison between model-based and model-free approaches. *PLoS One.* **9**, e89463 (2014)
42. Javorka, M., Trunkvalterova, Z., Tonhajzerova, I., Javorkova, J., Javorka, K., Baumert, M.: Short-term heart rate complexity is reduced in patients with type 1 diabetes mellitus. *Clin. Neurophysiol.* **119**, 1071–1081 (2008)
43. Bär, K.J., Boettger, M.K., Koschke, M., Schulz, S., Chokka, P., Yeragani, V.K., et al.: Non-linear complexity measures of heart rate variability in acute schizophrenia. *Clin. Neurophysiol.* **118**, 2009–2015 (2007)
44. Schulz, S., Koschke, M., Bär, K.J., Voss, A.: The altered complexity of cardiovascular regulation in depressed patients. *Physiol. Meas.* **31**, 303–321 (2010)
45. Schulz, S., Ritter, J., Oertel, K., Witt, K., Bär, K.J., Guntinas-Lichius, O., et al.: Altered autonomic regulation as a cardiovascular risk marker for patients with sudden sensorineural hearing loss. *Otol. Neurotol.* **35**, 1720–1729 (2014)

46. Bari, V., Valencia, J.F., Vallverdu, M., Girardengo, G., Marchi, A., Bassani, T., et al.: Multiscale complexity analysis of the cardiac control identifies asymptomatic and symptomatic patients in long QT syndrome type I. *PLoS One*. **9**, e93808 (2014)
47. Baumert, M., Javorka, M., Seeck, A., Faber, R., Sanders, P., Voss, A.: Multiscale entropy and detrended fluctuation analysis of QT interval and heart rate variability during normal pregnancy. *Comput. Biol. Med.* **42**, 347–352 (2012)
48. Bär, K.J., Koschke, M., Berger, S., Schulz, S., Tancer, M., Voss, A., et al.: Influence of olanzapine on QT variability and complexity measures of heart rate in patients with schizophrenia. *J. Clin. Psychopharmacol.* **28**, 694–698 (2008)
49. Porta, A., Guzzetti, S., Montano, N., Pagani, M., Somers, V., Malliani, A., et al.: Information domain analysis of cardiovascular variability signals: evaluation of regularity, synchronisation and co-ordination. *Med. Biol. Eng. Comput.* **38**, 180–188 (2000)
50. Bär, K.J., Schuhmacher, A., Hofels, S., Schulz, S., Voss, A., Yeragani, V.K., et al.: Reduced cardio-respiratory coupling after treatment with nortriptyline in contrast to S-citalopram. *J. Affect. Disord.* **127**, 266–273 (2010)
51. Ebert, A., Jochum, T., Ritter, J., Boettger, M.K., Schulz, S., Voss, A., et al.: Does parasympathetic modulation prior to ECT treatment influence therapeutic outcome? *Prog. Neuro-Psychopharmacol. Biol. Psychiatry*. **34**, 1174–1180 (2010)
52. Faes, L., Porta, A., Rossato, G., Adami, A., Tonon, D., Corica, A., et al.: Investigating the mechanisms of cardiovascular and cerebrovascular regulation in orthostatic syncope through an information decomposition strategy. *Auton. Neurosci.* **178**, 76–82 (2013)
53. Hadamard, J.: Les surfaces à courbures opposées et leurs lignes géodésiques. *J. Math. Pures Appl. Ser. V*, 27–73 (1898)
54. Morse, M., Hedlund, G.A.: Symbolic dynamics. *Amer. J. Math.* **60**, 815–866 (1938)
55. Aizawa, Y.: Symbolic dynamics approach to intermittent chaos. *Prog. Theor. Phys.* **70**, 1249–1263 (1983)
56. Hao, B.L.: Elementary symbolic dynamics and chaos in dissipative systems. World Scientific Publishing, Singapore (1990)
57. Paulus, M.P., Geyer, M.A., Gold, L.H., Mandell, A.J.: Application of entropy measures derived from the ergodic theory of dynamical systems to rat locomotor behavior. *Proc. Natl. Acad. Sci. U. S. A.* **87**, 723–727 (1990)
58. Voss, A., Dietz, R., Fiehring, H., Kleiner, H.J., Kurths, J., Saperin, P., et al.: High resolution ECG, heart rate variability and nonlinear dynamics: tools for high risk stratification. *Comput. Cardiol.* 261–264 (1993)
59. Kurths, J., Voss, A., Saperin, P., Witt, A., Kleiner, H.J., Wessel, N.: Quantitative analysis of heart rate variability. *Chaos*. **5**, 88–94 (1995)
60. Voss, A., Hnatkova, K., Wessel, N., Kurths, J., Sander, A., Schirdewan, A., et al.: Multiparametric analysis of heart rate variability used for risk stratification among survivors of acute myocardial infarction. *Pacing Clin. Electrophysiol.* **21**, 186–192 (1998)
61. Voss, A., Schroeder, R., Truebner, S., Goernig, M., Figulla, H.R., Schirdewan, A.: Comparison of nonlinear methods symbolic dynamics, detrended fluctuation, and Poincare plot analysis in risk stratification in patients with dilated cardiomyopathy. *Chaos*. **17**, 015120 (2007)
62. Żebrowski, J.J., Popławska, W., Baranowski, R., Buchner, T.: Symbolic dynamics and complexity in a physiological time series. *Chaos, Solitons Fractals*. **11**, 1061–1075. %@ 0960–0779 (2000)
63. Shannon, C.E.: A mathematical theory of communication. *Bell Syst. Tech. J.* **27**, 379–423 and 623–656 (1948)
64. Rényi, A.: On measures of entropy and information. *Proc. Fourth Berkeley Symp. Math. Stat. Probability*. **1**, 547–561 (1961)
65. Wessel, N., Brückner, C., Malberg, H., Schumann, A., Reinsperger, F., Osterziel, K., et al.: Long-term symbolic dynamics for heart rate variability analysis in patients with dilated cardiomyopathy. *Computers in Cardiology*. **26**, 253–256 (1999)

66. Guzzetti, S., Borroni, E., Garbelli, P.E., Ceriani, E., Della Bella, P., Montano, N., et al.: Symbolic dynamics of heart rate variability: a probe to investigate cardiac autonomic modulation. *Circulation*. **112**, 465–470 (2005)
67. Porta, A., Faes, L., Mase, M., D’Addio, G., Pinna, G.D., Maestri, R., et al.: An integrated approach based on uniform quantization for the evaluation of complexity of short-term heart period variability: application to 24 h Holter recordings in healthy and heart failure humans. *Chaos*. **17**, 015117 (2007)
68. Heitmann, A., Huebner, T., Schroeder, R., Perz, S., Voss, A.: Multivariate short-term heart rate variability: a pre-diagnostic tool for screening heart disease. *Med. Biol. Eng. Comput.* **49**, 41–50 (2011)
69. Voss, A., Schroeder, R., Caminal, P., Vallverdú, M., Brunel, H., Cygankiewicz, I., et al.: Segmented symbolic dynamics for risk stratification in patients with ischemic heart failure. *Cardiovasc. Eng. Technol.* **1**, 290–298 (2010)
70. Cysarz, D., Van Leeuwen, P., Edelhauser, F., Montano, N., Somers, V.K., Porta, A.: Symbolic transformations of heart rate variability preserve information about cardiac autonomic control. *Physiol. Meas.* **36**, 643–657 (2015)
71. Schulz, S., Adochiei, F.C., Edu, I.R., Schroeder, R., Costin, H., Bär, K.J., et al.: Cardiovascular and cardiorespiratory coupling analyses: a review. *Philos. Trans. A Math. Phys. Eng. Sci.* **371**, 20120191 (2013)
72. Baumert, M., Baier, V., Truebner, S., Schirdewan, A., Voss, A.: Short- and long-term joint symbolic dynamics of heart rate and blood pressure in dilated cardiomyopathy. *I.E.E.E. Trans. Biomed. Eng.* **52**, 2112–2115 (2005)
73. Schulz, S., Tupaika, N., Berger, S., Haueisen, J., Bär, K.J., Voss, A.: Cardiovascular coupling analysis with high-resolution joint symbolic dynamics in patients suffering from acute schizophrenia. *Physiol. Meas.* **34**, 883–901 (2013)
74. Kabir, M.M., Saint, D.A., Nalivaiko, E., Abbott, D., Voss, A., Baumert, M.: Quantification of cardiorespiratory interactions based on joint symbolic dynamics. *Ann. Biomed. Eng.* **39**, 2604–2614 (Oct 2011)
75. Baumert, M., Javorka, M., Kabir, M.: Joint symbolic dynamics for the assessment of cardiovascular and cardiorespiratory interactions. *Philos. Trans. A Math. Phys. Eng. Sci.* **373**, 20140097 (2015)
76. Schulz, S., Bär, K.J., Voss, A.: Analyses of heart rate, respiration and cardiorespiratory coupling in patients with schizophrenia. *Entropy*. **17**, 483–501 (2015)
77. Schulz, S., Haueisen, J., Bär, K.J., Voss, A.: Quantification of cardiorespiratory coupling in acute schizophrenia applying high resolution joint symbolic dynamics. In: *Computing in Cardiology Conference (CinC)*, pp. 101–104. Zaragoza, Spain (2013)
78. Bertinieri, G., Di Rienzo, M., Cavallazzi, A., Ferrari, A.U., Pedotti, A., Mancina, G.: Evaluation of baroreceptor reflex by blood pressure monitoring in unanesthetized cats. *Am. J. Phys.* **254**, H377–H383 (1988)
79. Laude, D., Elghozi, J.L., Girard, A., Bellard, E., Bouhaddi, M., Castiglioni, P., et al.: Comparison of various techniques used to estimate spontaneous baroreflex sensitivity (the EuroBaVar study). *Am. J. Phys. Regul. Integr. Comp. Phys.* **286**, R226–R231 (2004)
80. Schulz, S., Adochiei, F.C., Edu, I.R., Schroeder, R., Costin, H., Bar, K.J., et al.: Cardiovascular and cardiorespiratory coupling analyses: a review. *Philos. Trans. A Math. Phys. Eng. Sci.* **371**, 20120191 (2013)
81. Porta, A., Marchi, A., Bari, V., Heusser, K., Tank, J., Jordan, J., et al.: Conditional symbolic analysis detects nonlinear influences of respiration on cardiovascular control in humans. *Philos. Trans. A Math. Phys. Eng. Sci.* **373**, 20140096 (2015)
82. Bari, V., Marchi, A., De Maria, B., Rossato, G., Nollo, G., Faes, L., et al.: Nonlinear effects of respiration on the crosstalk between cardiovascular and cerebrovascular control systems. *Philos. Trans. A Math. Phys. Eng. Sci.* **374**, 20150179 (2016)
83. Wessel, N., Suhrbier, A., Riedl, M., Marwan, N., Malberg, H., Bretthauer, G., et al.: Detection of time-delayed interactions in biosignals using symbolic coupling traces. *EPL*. **87**, 10004 (2009)

84. Suhrbier, A., Riedl, M., Malberg, H., Penzel, T., Bretthauer, G., Kurths, J., et al.: Cardiovascular regulation during sleep quantified by symbolic coupling traces. *Chaos*. **20**, 045124 (2010)
85. Schulz, S., Voss, A.: Cardiovascular and cardiorespiratory coupling analysis—State of the art and future perspectives, In: 2014 8th Conference of the European Study Group on Cardiovascular Oscillations (ESGCO), Trento, pp. 25–26. (2014).
86. Mourot, L., Bouhaddi, M., Perrey, S., Rouillon, J.D., Regnard, J.: Quantitative Poincare plot analysis of heart rate variability: effect of endurance training. *Eur. J. Appl. Physiol.* **91**, 79–87 (2004)
87. Stein, P.K., Domitrovich, P.P., Huikuri, H.V., Kleiger, R.E.: Traditional and nonlinear heart rate variability are each independently associated with mortality after myocardial infarction. *J. Cardiovasc. Electrophysiol.* **16**, 13–20 (2005)
88. T. Mäkikallio, Analysis of heart rate dynamics by methods derived from nonlinear mathematics: clinical applicability and prognostic significance: Oulun Yliopisto, 1998.
89. Voss, A., Kurths, J., Kleiner, H.J., Witt, A., Saparin, P., Dietz, R., et al.: New methods for the detection of high risk patients in cardiology. *Biomed. Tech. (Berl)*. **39**, 134–143 (1994)
90. Seeck, A., Baumert, M., Fischer, C., Khandoker, A., Faber, R., Voss, A.: Advanced Poincare plot analysis differentiates between hypertensive pregnancy disorders. *Physiol. Meas.* **32**, 1611–1622 (2011)
91. Fischer, C., Voss, A.: Three-dimensional segmented Poincare plot analyses SPPA3 investigates cardiovascular and cardiorespiratory couplings in hypertensive pregnancy disorders. *Front. Bioeng. Biotechnol.* **2**, 51 (2014)
92. Karmakar, C.K., Khandoker, A.H., Gubbi, J., Palaniswami, M.: Complex correlation measure: a novel descriptor for Poincare plot. *Biomed. Eng. Online*. **8**, 17 (2009)
93. Lerma, C., Infante, O., Perez-Grovas, H., Jose, M.V.: Poincare plot indexes of heart rate variability capture dynamic adaptations after haemodialysis in chronic renal failure patients. *Clin. Physiol. Funct. Imaging*. **23**, 72–80 (2003)
94. Li, M., Vitányi, P.M.B.: An introduction to kolmogorov complexity and its applications. Springer Publishing Company, Inc., Heidelberg (1997)
95. Baumert, M., Baier, V., Voss, A., Brechtel, L., Haueisen, J.: Estimating the complexity of heart rate fluctuations—an approach based on compression entropy. *Fluct. Noise Lett.* **5**, L557–L563 (Dec 2005)
96. Truebner, S., Cygankiewicz, I., Schroeder, R., Baumert, M., Vallverdu, M., Caminal, P., et al.: Compression entropy contributes to risk stratification in patients with cardiomyopathy. *Biomed. Tech. (Berl)*. **51**, 77–82 (2006)
97. Costa, M., Goldberger, A.L., Peng, C.K.: Multiscale entropy analysis of complex physiologic time series. *Phys. Rev. Lett.* **89**, 068102 (2002)
98. Schumann, A., Schulz, S., Voss, A., Scharbrodt, S., Baumert, M., Bär, K.-J.: Baroreflex coupling assessed by cross-compression entropy. *Front. Physiol.* **8**, 282 (2017)
99. Granger, C.W.J.: Investigating causal relations by econometric models and cross-spectral methods. *Econometrica*. **37**, 424–438 (1969)
100. Novak, V., Novak, P., de Champlain, J., Le Blanc, A.R., Martin, R., Nadeau, R.: Influence of respiration on heart rate and blood pressure fluctuations. *J. Appl. Physiol.* (1985). **74**, 617–626 (1993)
101. Schulz, S., Bär, K.J., Voss, A.: Respiratory variability and cardiorespiratory coupling analyses in patients suffering from schizophrenia and their healthy first-degree relatives. *Biomed. Tech. (Berl)*. **57**(Suppl. 1), 1044 (2012)
102. Bär, K.J., Rachow, T., Schulz, S., Bassarab, K., Haufe, S., Berger, S., et al.: The phrenic component of acute schizophrenia—a name and its physiological reality. *PLoS One*. **7**, e33459 (2012)
103. Voss, A., Schulz, S., Schroeder, R., Baumert, M., Caminal, P.: Methods derived from nonlinear dynamics for analysing heart rate variability. *Philos. Trans. A Math. Phys. Eng. Sci.* **367**, 277–296 (2009)

104. Voss, A., Schulz, S., Schroder, R.: Analysis of cardiovascular oscillations using nonlinear dynamics methods for an enhanced diagnosis of heart and neurological diseases and for risk stratification. In: E-Health and Bioengineering Conference (EHB), vol. 2011, pp. 1–6 (2011)
105. Peupelmann, J., Boettger, M.K., Ruhland, C., Berger, S., Ramachandraiah, C.T., Yeragani, V.K., et al.: Cardio-respiratory coupling indicates suppression of vagal activity in acute schizophrenia. *Schizophr. Res.* **112**, 153–157 (2009)
106. Schulz, S., Bar, K.J., Voss, A.: Respiratory variability and cardiorespiratory coupling analyses in patients suffering from schizophrenia and their healthy first-degree relatives. *Biomed. Tech. (Berl)*. **57**, 1044 (2012)
107. Homma, I., Masaoka, Y.: Breathing rhythms and emotions. *Exp. Physiol.* **93**, 1011–1021 (2008)
108. Williams, L.M., Das, P., Harris, A.W., Liddell, B.B., Brammer, M.J., Olivieri, G., et al.: Dysregulation of arousal and amygdala-prefrontal systems in paranoid schizophrenia. *Am. J. Psychiatry*. **161**, 480–489 (2004)
109. Boiten, F.A., Frijda, N.H., Wientjes, C.J.: Emotions and respiratory patterns: review and critical analysis. *Int. J. Psychophysiol.* **17**, 103–128 (1994)
110. Weiden, P.J., Weiden, M.: Schizophrenia and respiratory symptoms: a serious, but overlooked, comorbidity. *CNS Spectr.* **15**, 10–13 (2010)
111. Goodwin, R., Lyons, J.S., McNally, R.J.: Panic attacks in schizophrenia. *Schizophr. Res.* **58**, 213–220 (Dec 1 2002)
112. Buckley, P.F., Miller, B.J., Lehrer, D.S., Castle, D.J.: Psychiatric comorbidities and schizophrenia. *Schizophr. Bull.* **35**, 383–402 (2009)
113. Porta, A., Di Rienzo, M., Wessel, N., Kurths, J.: Addressing the complexity of cardiovascular regulation. *Philos. Transact. A Math. Phys. Eng. Sci.* **367**, 1215–1218 (2009)
114. Voss, A., Seeck, A., Israel, A.K., Bar, K.J.: Enhanced spectral analysis of blood flow during post-occlusive reactive hyperaemia test in different tissue depths. *Auton. Neurosci.* **178**, 15–23 (2013)
115. Voss, A., Goernig, M., Schroeder, R., Truebner, S., Schirdewan, A., Figulla, H.R.: Blood pressure variability as sign of autonomic imbalance in patients with idiopathic dilated cardiomyopathy. *Pacing Clin. Electrophysiol.* **35**, 471–479 (2012)
116. Glass, L.: Chaos and heart rate variability. *J. Cardiovasc. Electrophysiol.* **10**, 1358–1360 (1999)
117. Porta, A., Castiglioni, P., Di Rienzo, M., Bari, V., Bassani, T., Marchi, A., et al.: Short-term complexity indexes of heart period and systolic arterial pressure variabilities provide complementary information. *J. Appl. Physiol.* **113**, 1810–1820 (2012)
118. Porta, A., Castiglioni, P., Di Rienzo, M., Bassani, T., Bari, V., Faes, L., et al.: Cardiovascular control and time domain Granger causality: insights from selective autonomic blockade. *Philos. Trans. A Math. Phys. Eng. Sci.* **371**, 20120161 (2013)
119. Baccala, L.A., de Brito, C.S., Takahashi, D.Y., Sameshima, K.: Unified asymptotic theory for all partial directed coherence forms. *Philos. Trans. A Math. Phys. Eng. Sci.* **371**, 20120158 (2013)
120. Blinowska, K.J., Kaminski, M., Brzezicka, A., Kaminski, J.: Application of directed transfer function and network formalism for the assessment of functional connectivity in working memory task. *Philos. Trans. A Math. Phys. Eng. Sci.* **371**, 20110614 (2013)

Complexity and Nonlinearity in Cardiovascular Signals

Barbieri, R.; Scilingo, E.P.; Valenza, G. (Eds.)

2017, VIII, 537 p. 133 illus., 72 illus. in color., Hardcover

ISBN: 978-3-319-58708-0